**Journal of Environmental Ecology**

https://jee.cultechpub.com/jee

E-ISSN: 3093-8074

Vol.2, No.1, March 2026

DOI: 10.64229/7j1ysx89

*Article*

# Spatiotemporal Patterns of Vegetation Greenness Dynamics Across India (2001-2023): A Harmonic Analysis of MODIS NDVI Time Series

**Satyam Shah***

School of Geography, Geology and the Environment, University of Leicester, University Road, LE1 7RH, Leicester, United Kingdom

*Corresponding author: Satyam Shah, satyamshah444@gmail.com

**Abstract**

Vegetation greenness dynamics serve as sensitive indicators of ecosystem health and environmental change. This study employs harmonic regression analysis of Moderate Resolution Imaging Spectroradiometer (MODIS) Normalized Difference Vegetation Index (NDVI) time series to detect and quantify changes in seasonal vegetation patterns across India over two decades (2001-2023). Two periods early (2001-2011) and recent (2013-2023) were compared across 36 states and 11 biome types using three harmonic parameters: mean greenness, seasonality amplitude, and peak timing phase. Analysis of 10.2 million valid pixels at 500 m resolution reveals a decline in mean NDVI of 0.028 (Cohen's d = 0.18), with 57.6% of vegetated pixels showing reduced greenness. Mann-Kendall trend analysis confirmed this pattern with 91.7% method concordance. At the state level, 75% of administrative units showed declining greenness, with northeastern states experiencing the most severe reductions (0.13-0.24 NDVI units). EVI validation in high-biomass regions confirmed that declines persist across both indices ($r = 0.874$), indicating that NDVI saturation effects are modest (~10%) and do not alter the primary findings. Among biomes, mangroves exhibited the greatest loss (−0.115), while deserts and xeric shrublands showed marginal increases (+0.027). Land cover stratification revealed forests experienced the strongest decline (−0.052) whereas croplands showed modest increases (+0.011), supporting land use change as a primary driver. Climate correlations at the state level identified vapor pressure deficit change ($r = −0.512$, $p = 0.002$) and precipitation change ($r = 0.449$, $p = 0.006$) as significant predictors, and a strong inverse relationship between baseline vegetation density and subsequent change ($r = −0.550$, $p < 0.001$) indicates that well-vegetated areas are disproportionately degrading. This Google Earth Engine–based harmonic framework provides a reproducible approach for continental-scale vegetation monitoring and ecosystem assessment.

**Keywords**

Vegetation dynamics, Harmonic analysis, Normalized difference vegetation index, Seasonal greenness, Remote sensing, Ecosystem change, India

**Article History**

Received: 08 February 2026
Revised: 10 April 2026
Accepted: 06 May 2026
Available Online: 13 May 2026

## 1. Introduction

Vegetation phenology, defined as the timing and progression of recurring biological events such as leaf emergence, peak greenness, and senescence, is widely recognized as a fundamental indicator of ecosystem functioning and environmental change [1,2]. Shifts in phenological patterns can cascade through ecological systems, affecting nutrient cycling, carbon sequestration, species interactions, and ecosystem productivity [3]. Satellite-based monitoring of vegetation dynamics over extended temporal scales has become indispensable for understanding how terrestrial ecosystems respond to climate variability, land use change, and anthropogenic pressures [4,5]. The Normalized Difference Vegetation Index (NDVI), first proposed by Tucker [6], remains one of the most widely utilized spectral indices for characterizing vegetation dynamics, owing to its sensitivity to chlorophyll content and canopy structure.

Over the past two decades, numerous studies have documented significant changes in vegetation greenness at regional and global scales. While some studies provided early evidence of increased plant growth in northern high latitudes [7] and widespread greening driven by $CO_2$ fertilization, nitrogen deposition, and climate change [8], these global trends mask substantial regional heterogeneity. Many areas experience persistent declines in vegetation greenness due to drought stress, deforestation, and land degradation [9,10]. Recent assessments have shown complex global patterns, with vegetation greenness in 2023 exhibiting both regional gains and losses linked to climate extremes [11], and projections suggesting that observed advancements in spring vegetation phenology across the Northern Hemisphere may reverse after 2060 under moderate warming scenarios [12]. Understanding the spatial patterns and drivers of vegetation change at the regional level is therefore essential for developing targeted conservation and land management strategies.

Satellite remote sensing provides the only practical means of monitoring vegetation continuously across large spatial extents [13]. The Moderate Resolution Imaging Spectroradiometer (MODIS) aboard National Aeronautics and Space Administration (NASA)'s Terra satellite has generated a consistent, near-daily record of global vegetation conditions since 2000, making it one of the most valuable datasets for long-term vegetation research [14]. The MODIS Vegetation Index product (MOD13A1) provides 16-day composite NDVI imagery at 500 m spatial resolution, with built-in quality assurance information that enables filtering of cloud-contaminated and otherwise unreliable observations [15,16].

Several analytical approaches have been developed to extract temporal patterns from satellite time series. Threshold-based methods identify transition dates by detecting when vegetation indices cross predefined values [14], while curve-fitting techniques employ logistic or polynomial functions to model seasonal trajectories [17]. Among these approaches, harmonic regression, also termed Fourier analysis or spectral decomposition, offers distinct advantages for characterizing seasonal vegetation patterns [18,19]. By decomposing temporal variation into periodic components, harmonic analysis extracts physically interpretable parameters including mean vegetation condition, seasonality strength (amplitude), and timing of peak greenness (phase), without requiring assumptions about the shape of the seasonal curve [18]. This approach has been widely validated for modeling vegetation dynamics from NDVI time series across diverse geographical regions [20,21], including applications in European temperate forests and grasslands [22] and West African rangelands [23]. The advent of cloud computing platforms, particularly Google Earth Engine (GEE), has transformed the capacity for large-scale remote sensing analysis by enabling access to petabyte-scale archives and distributed computing resources [24,25].

India presents a uniquely compelling setting for vegetation research due to its exceptional ecological diversity and the intensity of environmental pressures it faces. Spanning approximately 3.29 million $km^2$, the country encompasses 11 terrestrial biomes ranging from tropical moist broadleaf forests in the Western Ghats and northeast to deserts and xeric shrublands in the northwest, with temperate and alpine ecosystems in the Himalayas [26]. This bioclimatic gradient is further shaped by the Indian monsoon system, which generates one of the strongest seasonal vegetation cycles on Earth [27]. India has experienced substantial environmental change in recent decades, with the India State of Forest Report 2023 documenting mixed trends including overall increases in forest and tree cover masked by significant losses in dense forest areas [28]. Forest cover dynamics have been shaped by competing forces of deforestation, particularly in the northeast, and afforestation programs in degraded areas [29,30]. Recent assessments have documented widespread vegetation degradation across India [31] and identified complex climate drivers of ecosystem change [32]. Agricultural intensification, supported by expanding irrigation infrastructure, has transformed vegetation patterns in northwestern states [31,33,34], while rapid urbanization has led to significant vegetation loss around major cities [32,35]. Climate trends over India include changes in monsoon precipitation patterns, increased frequency of extreme weather events, and warming temperatures, all of which have implications for vegetation dynamics [36,37].

Despite these pressures, comprehensive analyses of long-term vegetation change across India's diverse ecosystems using consistent satellite-based approaches remain limited. Most existing studies have focused on specific regions, land cover types, or shorter time periods [38,39]. The critical gap lies in the absence of integrated, national-scale analyses that (1) utilize harmonic regression to characterize both magnitude and seasonal structure of vegetation change, (2) extend beyond simple greenness trends to examine seasonal amplitude and timing shifts, (3) systematically compare patterns across administrative units and natural biomes, and (4) evaluate relationships with climatic drivers at scales relevant to policy and management decisions.

This study addresses these gaps by applying harmonic regression analysis to a 23-year MODIS NDVI time series (2001-2023) to quantify changes in seasonal vegetation patterns across India at both pixel and administrative scales. The specific objectives are to (1) quantify changes in mean vegetation greenness, seasonality amplitude, and peak timing between early (2001-2011) and recent (2013-2023) periods, (2) assess the magnitude and spatial distribution of vegetation change at the national level, (3) identify the biomes and regions exhibiting the greatest vegetation sensitivity, (4) evaluate correlations between observed vegetation changes and climate variables, and (5) demonstrate the utility of harmonic parameters as indicators of ecosystem change. While the harmonic parameters employed in this study (mean NDVI, amplitude, and phase) reflect seasonal vegetation greenness patterns rather than discrete phenological events (e.g., specific leaf-out dates or senescence onset), they nonetheless provide ecologically meaningful characterization of vegetation seasonal dynamics and long-term change. The analysis is implemented entirely within GEE, ensuring reproducibility and scalability for ongoing monitoring applications.

## 2. Materials and Methods

### 2.1 Study Area

The study encompasses the entire terrestrial extent of India (approximately 6°N to 37°N latitude, 68°E to 98°E longitude), covering an area of approximately 3.29 million km$^2$ across 36 states and union territories. India's vegetation is distributed across 11 biomes as classified by the RESOLVE Ecoregions dataset [26], including tropical moist and dry broadleaf forests, tropical and temperate grasslands, montane shrublands, deserts, mangroves, and coniferous forests. The climate is dominated by the Indian monsoon, with a pronounced wet season (June to September) driving a strong seasonal vegetation cycle across most of the subcontinent [27]. Administrative boundaries were obtained from the Database of Global Administrative Areas (GADM) version 4.1 (2022), which provides the current delineation of all 36 states and union territories including the 2019 reorganization of Jammu and Kashmir and Ladakh as separate union territories (Figure 1).

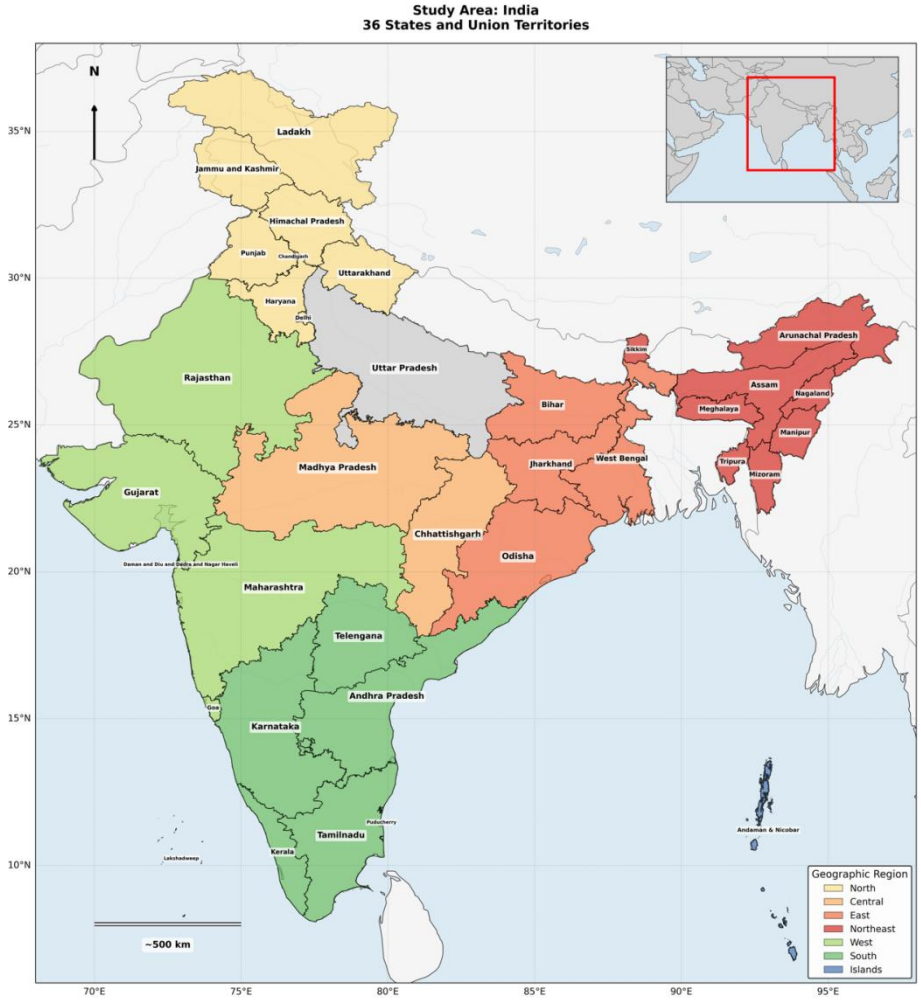


**Figure 1.** Study area map of India's 36 states and union territories analysed in this study, colour-coded by geographic region (North, Central, East, Northeast, West, South, and Islands). State and union territory names are labelled. The inset shows the location of India within South Asia. Administrative boundaries are derived from the Database of Global Administrative Areas (GADM) version 4.1 (2022).

### 2.2 Satellite Data and Preprocessing

MODIS NDVI data were obtained from the MOD13A1 Version 6.1 product [15], which provides 16-day maximum value composite NDVI at 500 m spatial resolution. The dataset was accessed through the GEE platform [24] for the period 1 January 2001 to 31 December 2023, yielding 253 composite images per analysis period. The NDVI values, stored as integer values in the original product, were rescaled by a factor of 0.0001 to obtain values in the standard range.

Quality filtering was performed using the SummaryQA band included in the MOD13A1 product. Only pixels flagged as good quality (SummaryQA = 0) or marginal quality (SummaryQA = 1) were retained for analysis. Pixels classified as snow/ice-covered (SummaryQA = 2) or cloudy (SummaryQA = 3) were masked. This quality filtering approach follows established protocols for MODIS NDVI time series analysis [14,40]. A land mask was applied to exclude non-vegetated areas from the analysis. Pixels with mean NDVI below 0.1 in both analysis periods were excluded, effectively removing permanent water bodies, barren lands, and built-up areas with minimal vegetation. Island territories including Andaman and Nicobar Islands and Lakshadweep were included in the analysis where sufficient valid observations were available after quality filtering. High-altitude regions above 5000 m elevation, predominantly in Ladakh and northern Himachal Pradesh, were retained but exhibited lower observation density due to persistent snow cover and cloud contamination.

### 2.3 Harmonic Regression Model

Harmonic regression was employed to decompose the NDVI time series into interpretable seasonal components. The model expresses NDVI as a function of time using sinusoidal terms representing periodic vegetation cycles [18,19]. This approach has been widely validated for modeling vegetation dynamics from NDVI time series across diverse geographical regions [20,21,41,42]. For each pixel, the following model was fitted:

$$NDVI(t) = \beta_0 + \beta_1 t + \sum_{k=1}^{2}\left[a_k \cos\left(\frac{2\pi k t}{T}\right) + b_k \sin\left(\frac{2\pi k t}{T}\right)\right] + \varepsilon \quad (1)$$

where NDVI(t) is the observed NDVI at time t (expressed in fractional years since 1 January 1970), $\beta_0$ is the intercept representing the temporal mean NDVI, $\beta_1$ is the linear trend coefficient, $a_k$ and $b_k$ are the cosine and sine coefficients for the kth harmonic respectively, T is the annual period (1 year), and ε is the residual error. Two harmonic terms (k = 1, 2) were included: the first harmonic captures the dominant annual cycle, while the second captures semi-annual variations associated with bimodal growing seasons observed in parts of peninsular India. The use of two harmonic terms provides flexibility to represent both unimodal phenological cycles (dominant in northern and northeastern India) and bimodal cycles (occurring in southern regions with distinct monsoon and post-monsoon growing periods) [43,44].

From the fitted coefficients of the first harmonic, two ecologically interpretable parameters were derived. The amplitude (A), representing the strength of seasonal vegetation variation, was calculated as:

$$A = \sqrt{a_1^2 + b_1^2} \quad (2)$$

The phase ($\varphi$), representing the timing of peak annual greenness, was calculated as:

$$\varphi = \arctan\left(\frac{b_1}{a_1}\right) \quad (3)$$

where arctan2 is the two-argument arctangent function that preserves quadrant information, yielding phase values in the range from negative π to positive π radians.

The phase difference between periods was calculated using circular statistics to account for the periodic nature of angular data [45]. For each pixel, the phase shift was computed as:

$$\Delta\varphi = \text{angle}\left(e^{i\varphi_{recent}} \cdot e^{-i\varphi_{early}}\right) \quad (4)$$

This approach ensures that phase differences are constrained to the interval from negative π to positive π, correctly handling cases where the phase wraps around the annual cycle boundary. The phase value in radians was subsequently converted to calendar days for ecological interpretation:

$$\Delta_{\text{days}} = \frac{\triangle\varphi}{2\pi} \times 365 \quad (5)$$

A positive phase shift indicates a delay in peak greenness (later in the calendar year), while a negative shift indicates advancement (earlier peak).

The model was fitted independently for each pixel using ordinary least squares regression, implemented via the linearRegression reducer in GEE [24]. The six independent variables (constant, time, cos1, sin1, cos2, sin2) were

regressed against the dependent variable (NDVI) for each pixel across all available composite images within each period.

### 2.4 Temporal Analysis Framework

The 23-year study period was divided into two sub-periods: the early period (2001–2011) and the recent period (2013–2023), each comprising 11 years and approximately 253 composite images. A one-year buffer (2012) was excluded to ensure clear temporal separation between periods, minimize transitional effects, and maintain equal period lengths for direct comparability. This two-period comparative approach was chosen over continuous trend analysis for several reasons: (1) it provides a clear temporal baseline for change assessment relevant to policy evaluation, (2) it reduces sensitivity to short-term interannual variability that can complicate linear trend interpretation, (3) it facilitates straightforward before-after comparison of harmonic parameters, and (4) the 11-year periods are sufficiently long to characterize stable seasonal patterns while being short enough to detect decadal-scale changes. While this approach does not capture nonlinear dynamics or abrupt changes occurring within periods, it provides robust characterization of average conditions and their change [44].

The harmonic regression model (Equation 1) was fitted independently for each period, yielding separate estimates of mean NDVI ($\beta_0$), amplitude (A), and phase ($\varphi$) for the early and recent periods. Vegetation change was then quantified as the difference between the recent and early period parameters:

$$\Delta\text{Mean}=\beta_0^{\text{recent}} - \beta_0^{\text{early}} \tag{6}$$

$$\Delta\text{Amplitude} = A^{\text{recent}} - A^{\text{early}} \tag{7}$$

$$\Delta\text{Phase} = \varphi^{\text{recent}} - \varphi^{\text{early}} \tag{8}$$

with phase difference calculated using circular statistics as described in Equation 4.

A comprehensive validity mask was applied to exclude unreliable pixels. Pixels were retained only if NDVI values in both periods fell within the range 0 to 1, amplitude values were below 0.5, the absolute change in mean NDVI was below 0.5, and the absolute phase shift was below 183 days (half a year). These thresholds exclude physically implausible values arising from insufficient valid observations or fitting failures.

### 2.5 Zonal Statistical Analysis

Phenological parameters and change metrics were aggregated at two spatial scales: administrative units (36 states and union territories) and biome types (11 biomes present in India). Administrative boundaries were derived from the Database of Global Administrative Areas (GADM) version 4.1 (2022), which provides the current delineation of all 36 states and union territories including the 2019 reorganization of Jammu and Kashmir and Ladakh as separate union territories. Biome classification was obtained from the RESOLVE Ecoregions 2017 dataset [26], rasterized to 500 m resolution to match the MODIS data.

For each spatial unit, area-weighted mean values of all phenological parameters were extracted from the pixel-level raster data using zonal statistics operations. Specifically, for each state or biome j, the mean parameter value was calculated as:

$$X_j = \frac{\sum_{i \in j} X_i \cdot A_i}{\sum_{i \in j} A_i} \tag{9}$$

where X_i is the parameter value for pixel i, A_i is the area of pixel i (accounting for latitudinal variation in pixel size), and the summation is over all valid pixels within unit j. This approach ensures that larger homogeneous areas contribute proportionally more to the unit mean than fragmented edge pixels.

### 2.6 Climate Data and Correlation Analysis

Climate data were obtained from the European Centre for Medium-Range Weather Forecasts (ECMWF) Reanalysis v5 (ERA5)-Land monthly aggregated dataset [46] accessed through GEE. Four climate variables were calculated for both the early and recent periods:

(1) Mean 2 m air temperature (°C)

(2) Total annual precipitation (mm/year)

(3) Mean vapor pressure deficit (kPa), calculated from temperature and dewpoint temperature as VPD = 0.611 × exp[(17.27 × T)/(T + 237.3)] × (1 – RH/100), where RH is relative humidity

(4) Soil moisture ($m^3/m^3$), volumetric water content in the 0 to 7 cm layer

Temporal changes were computed as the difference between recent and early period means. Climate variables were extracted at state level to match the spatial scale of the phenological analysis. The relationship between climate variables and vegetation change was evaluated using Pearson correlation coefficients. Twelve climate-phenology pairs were examined:

Change correlations: temperature change versus NDVI change, precipitation change versus NDVI change, VPD change versus NDVI change, soil moisture change versus NDVI change, temperature change versus amplitude change, and VPD change versus amplitude change. Baseline correlations: baseline temperature versus NDVI change, baseline precipitation versus NDVI change, baseline VPD versus NDVI change, baseline NDVI versus NDVI change, baseline NDVI versus amplitude change, and VPD change versus phase change. Statistical significance was assessed at $\alpha = 0.05$ and $\alpha = 0.01$ levels.

### 2.7 Statistical Significance Testing

Two complementary statistical approaches were employed. For pixel-level patterns, descriptive statistics and effect sizes were calculated to characterize the magnitude and direction of change, recognizing that with n approximately 10 million spatially autocorrelated pixels, traditional significance tests are uninformative due to pseudo-replication [47]. Instead, Cohen's d effect size for mean NDVI change was computed:

$$d = \frac{\bar{X}_{\text{recent}} + \bar{X}_{\text{early}}}{s_{\text{pooled}}} \tag{10}$$

where s_pooled is the pooled standard deviation across periods. Effect sizes were interpreted using conventional thresholds: absolute value of d less than 0.2 equals negligible, 0.2 to 0.5 equals small, 0.5 to 0.8 equals medium, greater than 0.8 equals large [48].

For state-level analysis (n = 36), where spatial units can reasonably be considered independent samples, formal statistical tests were conducted. Paired t-tests were used to compare early and recent period mean NDVI values across states. A one-sample t-test assessed whether the mean change in NDVI was significantly different from zero. The non-parametric Wilcoxon signed-rank test was additionally employed as a distribution-free alternative to confirm the robustness of the parametric results. All statistical analyses were performed in Python 3.12 using the SciPy library [34]. Standard deviations (SD) are reported throughout as measures of variability (not standard errors), unless otherwise noted.

### 2.8 Pixel-Wise Trend Analysis and Validation

To validate the two-period comparison approach and assess the consistency of vegetation change trajectories, complementary pixel-wise trend analysis was conducted using the non-parametric Mann-Kendall test and Theil-Sen slope estimator [49]. For each pixel with at least 80% valid observations across the full 23-year period, the following were calculated:

(1) Mann-Kendall $\tau$ statistic: a rank-based measure of monotonic trend direction and strength, with significance assessed at $\alpha = 0.05$ using a two-tailed test accounting for temporal autocorrelation [42].

(2) Theil-Sen slope: the median of all pairwise slopes between observation pairs, providing a robust estimate of NDVI change rate (NDVI units per year) resistant to outliers.

Trends were classified as significant increasing ($\tau > 0$, $p < 0.05$), significant decreasing ($\tau < 0$, $p < 0.05$), or non-significant. To assess consistency between the two analytical approaches, the concordance between two-period NDVI change direction and Mann-Kendall trend direction was calculated at both pixel and state levels.

### 2.9 Enhanced Vegetation Index Validation

To assess potential NDVI saturation effects in high-biomass regions, parallel analysis was conducted using the Enhanced Vegetation Index (EVI) from the same MOD13A1 product for a subset of high-NDVI states (baseline NDVI greater than 0.6) where saturation is most likely [40]. EVI employs a soil-adjusted canopy background and atmospheric resistance term that maintains sensitivity in dense vegetation:

$$\text{EVI} = 2.5 \times \frac{\text{NIR} - \text{Red}}{\text{NIR} + 6 \times \text{Red} - 7.5 \times \text{Blue} + 1} \tag{11}$$

For the seven northeastern states (Tripura, Mizoram, Nagaland, Meghalaya, Manipur, Assam, Arunachal Pradesh) plus the Western Ghats regions of Kerala and Karnataka, the same two-period change metrics were calculated using EVI and compared them with NDVI-based results. The EVI-NDVI correlation for change detection was assessed using Pearson correlation and Bland-Altman analysis to quantify systematic differences.

### 2.10 Land Cover Stratification Analysis

To assess whether observed vegetation changes differ systematically across land cover types, pixel-level results were stratified using the MODIS Land Cover Type product (MCD12Q1 Collection 6.1) [45]. The dominant land cover class for each pixel was extracted based on the International Geosphere-Biosphere Programme (IGBP) classification scheme from the year 2010 (midpoint of study period). Pixels were grouped into seven broad categories: (1) Forests (Evergreen Needleleaf, Evergreen Broadleaf, Deciduous Needleleaf, Deciduous Broadleaf, Mixed Forests), (2) Shrublands (Closed and Open Shrublands), (3) Savannas (Woody Savannas and Savannas), (4) Grasslands, (5) Croplands (including Cropland/Natural Vegetation Mosaic), (6) Urban and Built-up, and (7) Other (including wetlands and barren).

For each land cover category, the mean NDVI change, percentage of pixels showing decline, and mean Mann-Kendall trend slope were calculated. This stratification enables assessment of whether the observed decline signal is concentrated in forest areas (supporting land use change attribution) or distributed across all vegetation types (supporting climate driver attribution).

### 2.11 Spatial Autocorrelation Analysis

To address the pseudo-replication issue inherent in continental-scale pixel-based analysis, spatial autocorrelation in NDVI change was quantified using global Moran's I statistic [50]. Moran's I was calculated using a distance-based spatial weights matrix with a 50 km neighborhood distance (approximately 100 pixels at 500 m resolution):

$$I = \frac{n \sum_i \sum_j w_{ij} (x_i - \bar{x})(x_j - \bar{x})}{\left( \sum_i \sum_j w_{ij} \right) \sum (x_i - \bar{x})^2} \tag{12}$$

where n is the number of pixels, x_i is NDVI change for pixel i, $\bar{x}$ is the mean NDVI change, and w_ij is the spatial weight between pixels i and j.

From Moran's I, the effective sample size accounting for spatial dependence was estimated [51]:

$$n_{\mathrm{eff}} = \frac{n}{1 + (n-1) \times 1} \tag{13}$$

This effective sample size was used to recalculate appropriate significance thresholds and confidence intervals for pixel-based statistics.

### 2.12 Circular Statistical Analysis of Phase Shifts

To assess whether observed phase shifts represent statistically significant changes in peak greenness timing, circular statistical tests appropriate for angular data were applied [52]. For each state, the circular mean phase for early and recent periods was calculated and tested for significant difference using the Watson-Wheeler test for homogeneity of circular distributions [53]. The Rayleigh test was used to confirm non-uniformity of phase distributions (i.e., presence of a dominant seasonal peak). Circular mean phase was converted to day of year for ecological interpretation, and states with significant phase shifts ($p < 0.05$) were identified.

### 2.13 Data Processing Environment

All satellite data acquisition, harmonic regression analysis, and raster export operations were performed on the GEE cloud computing platform [24]. Raster data were exported as GeoTIFF files at 500 m resolution (phenological and biome data) and 5,000 m resolution (climate data). Post-processing, zonal statistics extraction, statistical testing, and figure generation were conducted locally using Python 3.12 with the Rasterio, GeoPandas, Rasterstats, NumPy, Pandas, SciPy, and Matplotlib libraries.

## 3. Results

### 3.1 National-Scale Vegetation Dynamics Across India

Harmonic regression analysis of 10.2 million valid MODIS NDVI pixels across India revealed a decline in mean vegetation greenness between the early (2001 to 2011) and recent (2013 to 2023) periods. The national mean NDVI decreased from 0.382 ± 0.219 (mean ± SD) to 0.354 ± 0.205, representing an absolute decline of 0.028 ± 0.157. This represents a small to moderate effect size (Cohen's d = 0.18).

Spatial autocorrelation analysis revealed strong positive autocorrelation in NDVI change (global Moran's I = 0.524, $p < 0.0001$), indicating that neighboring pixels tend to exhibit similar change patterns. This spatial structure reduces the effective independent sample size to approximately n_eff = 19,780, or 0.19% of the nominal 10.2 million pixels. When recalculated using the effective sample size, the national mean decline remains statistically distinguishable from zero (t

= 11.47, $p < 0.0001$), confirming that the result is not an artifact of pseudo-replication. The spatial clustering of positive and negative change areas (Figure 2) reflects coherent regional processes rather than random pixel-level noise.

Of the total valid pixels, 57.6% (5,879,037 pixels) exhibited declining greenness, while 42.4% (4,327,958 pixels) showed increases (Figure 2). At the state level, where spatial units can be treated as independent samples (n = 36), the mean NDVI change of 0.052 was statistically distinguishable from zero (paired t-test: $t = 4.123$, $p = 0.0002$; Wilcoxon signed-rank: $W = 110$, $p = 0.0003$). However, the ecological significance is better conveyed by the effect magnitude: three-quarters of states experienced declining greenness, with declines exceeding 0.10 NDVI units in seven states. Seasonality amplitude showed minimal overall change (early: $0.133 \pm 0.058$; recent: $0.134 \pm 0.058$; $\Delta = 0.001 \pm 0.022$), indicating that the strength of the annual vegetation cycle remained largely stable at the national scale despite the decline in mean greenness (Figure 3). Peak vegetation timing showed a marginal shift of $1.43 \pm 13.91$ days, with 60.0% of pixels exhibiting a later peak and 40.0% an earlier peak (Figure 4). Given the small magnitude relative to inter-pixel variability, this shift does not represent a consistent national-level trend, though substantial spatial heterogeneity was evident. A comprehensive summary of these parameters is provided in Table 1.

**Table 1.** Summary of phenological parameters across India (2001-2011 vs. 2013-2023).

| **Parameter** | **Period/Metric** | **Mean** | **SD** | |
|---|---|---|---|---|
| Mean NDVI | Early (2001-2011) | 0.382 | 0.219 | |
| Mean NDVI | Recent (2013-2023) | 0.354 | 0.205 | |
| Mean NDVI | Change (Δ) | –0.028 | 0.157 | |
| Amplitude | Early (2001-2011) | 0.133 | 0.058 | |
| Amplitude | Recent (2013-2023) | 0.134 | 0.058 | |
| Amplitude | Change (Δ) | +0.001 | 0.022 | |
| Peak Timing | Shift (Δ days) | +1.43 | 13.91 | |
| **Pixel Counts** | **Count** | | **Percentage** | |
| Total valid pixels | 10,206,995 | | 100.0% | |
| Greening pixels | 4,327,958 | | 42.4% | |
| Browning pixels | 5,879,037 | | 57.6% | |
| Earlier peak pixels | 4,082,697 | | 40.0% | |
| Later peak pixels | 6,124,298 | | 60.0% | |
| **Statistical Tests** | **Test Type** | **Statistic** | **p-value** | **Significance** |
| Paired t-test (NDVI) | | $t = 4.123$ | 0.0002 | ** |
| One-sample t-test ($\Delta \neq 0$) | | $t = -4.123$ | 0.0002 | ** |
| Wilcoxon signed rank | | $W = 110$ | 0.0003 | ** |
| Effect size ( Cohen's d) | 0.18 | | – | |
| Spatial autocorrelation (Moran's I) | 0.524 | | < 0.0001 | |
| Effective sample size | 19,780 | | – | |

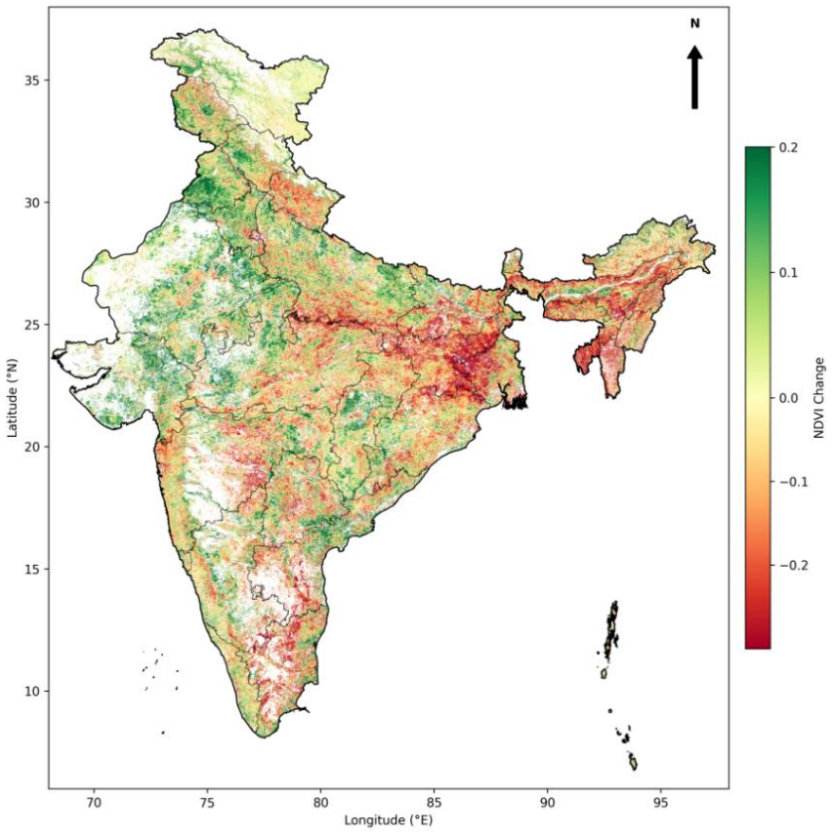


**Figure 2.** Spatial distribution of change in mean NDVI across India (2013-2023 minus 2001-2011). Green shading indicates greening (positive NDVI change) and red shading indicates browning (negative NDVI change). State boundaries are overlaid in black. Values range from –0.3 (browning) to +0.2 (greening), with white representing no change.

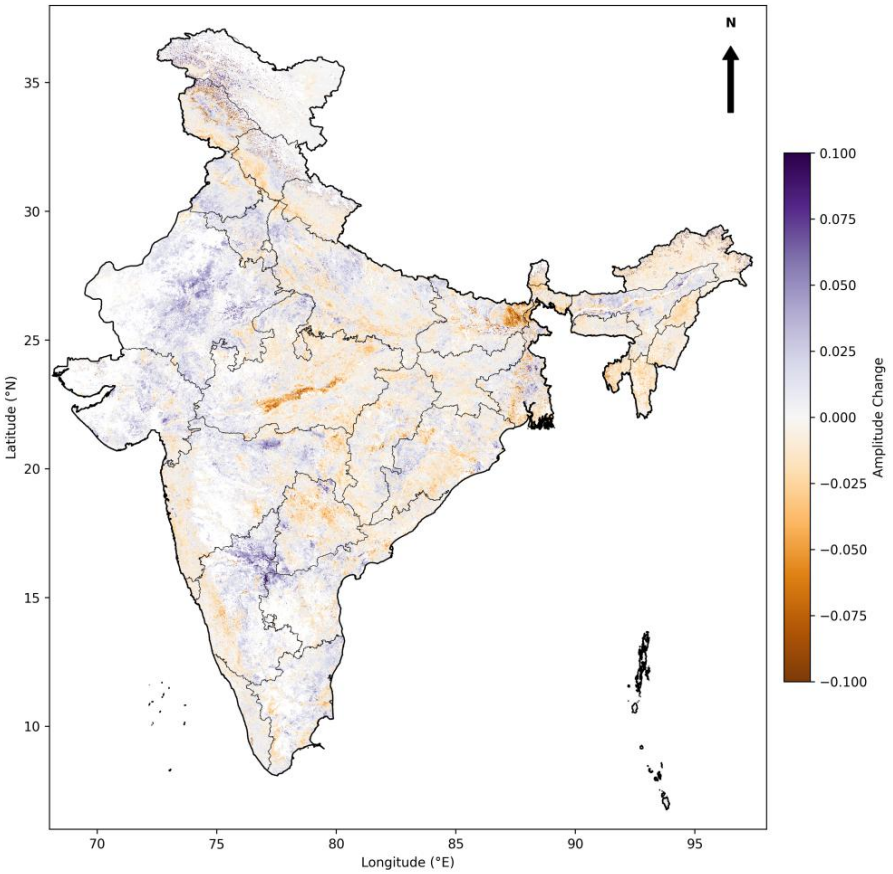


**Figure 3**. Spatial distribution of change in seasonality amplitude across India. Purple shading indicates increased seasonality and orange shading indicates decreased seasonality. Values range from –0.1 to +0.1, with white representing no change.

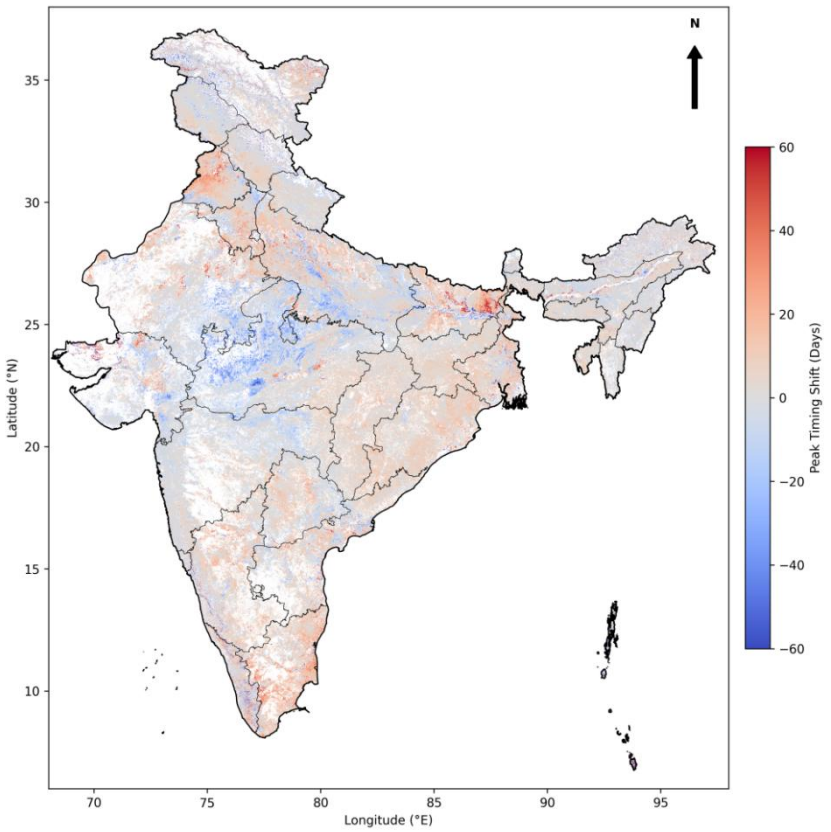


**Figure 4**. Spatial distribution of peak vegetation timing shift across India. Red shading indicates a shift toward a later peak and blue shading indicates a shift toward an earlier peak. Values range from –60 to +60 days, with white representing no change.

### 3.2 Temporal Comparison of Vegetation Greenness

Comparison of the spatial patterns of mean NDVI between the two periods revealed region-specific changes in vegetation condition (Figure 5). The early period exhibited higher NDVI values across the northeastern states, the Western Ghats, and parts of central India, while the recent period showed reduced greenness in these regions. Conversely, northwestern India, including Rajasthan, Gujarat, Punjab, and Haryana, displayed higher NDVI values in the recent period relative to the baseline. The Indo-Gangetic Plain showed a mixed pattern, with some areas exhibiting increases in greenness associated with intensive agriculture and others showing declines.

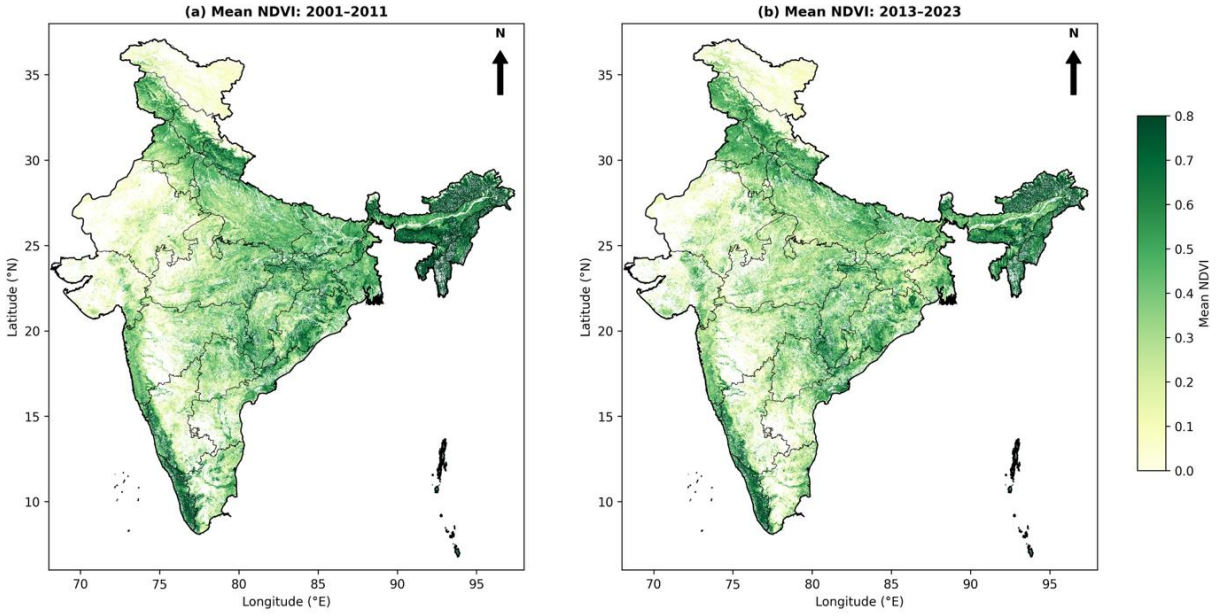


**Figure 5**. Temporal comparison of mean NDVI across India. (a) Mean NDVI for the early period (2001-2011). (b) Mean NDVI for the recent period (2013-2023). Values range from 0 (bare/sparse vegetation) to 0.8 (dense vegetation), displayed using a sequential yellow-to-green colour scheme.

### 3.3 State-Level Phenological Changes

At the state level, 27 of 36 administrative units (75.0%) exhibited a decline in mean NDVI, while 9 states (25.0%) showed increases (Figure 6). The mean state-level NDVI decreased from 0.476 ± 0.196 to 0.424 ± 0.167, with a mean change of 0.052 ± 0.076 (Table 2).

The most pronounced declines in vegetation greenness were observed in Tripura (Δ = –0.243), Jharkhand (Δ = –0.181), Mizoram (Δ = –0.166), Delhi (Δ = –0.144), and Nagaland (Δ = –0.134). These states are located predominantly in the northeastern region and include both forested areas and urban centers. The greatest increases in greenness were recorded in Punjab (Δ = 0.078), Gujarat (Δ = 0.076), Rajasthan (Δ = 0.064), Puducherry (Δ = 0.056), and Haryana (Δ = 0.048), all of which are characterized by either intensive irrigated agriculture or arid landscapes. Jammu and Kashmir (Δ = 0.003) and Ladakh (Δ = 0.016) exhibited marginal increases.

Small island union territories (Lakshadweep, portions of Andaman and Nicobar) had insufficient valid pixels after quality filtering and are excluded from state-level summary statistics. Manipur exhibited data gaps in portions of the early period due to persistent cloud cover during monsoon seasons; the reported change value (Δ = –0.091) is based on 68% spatial coverage and should be interpreted with caution.

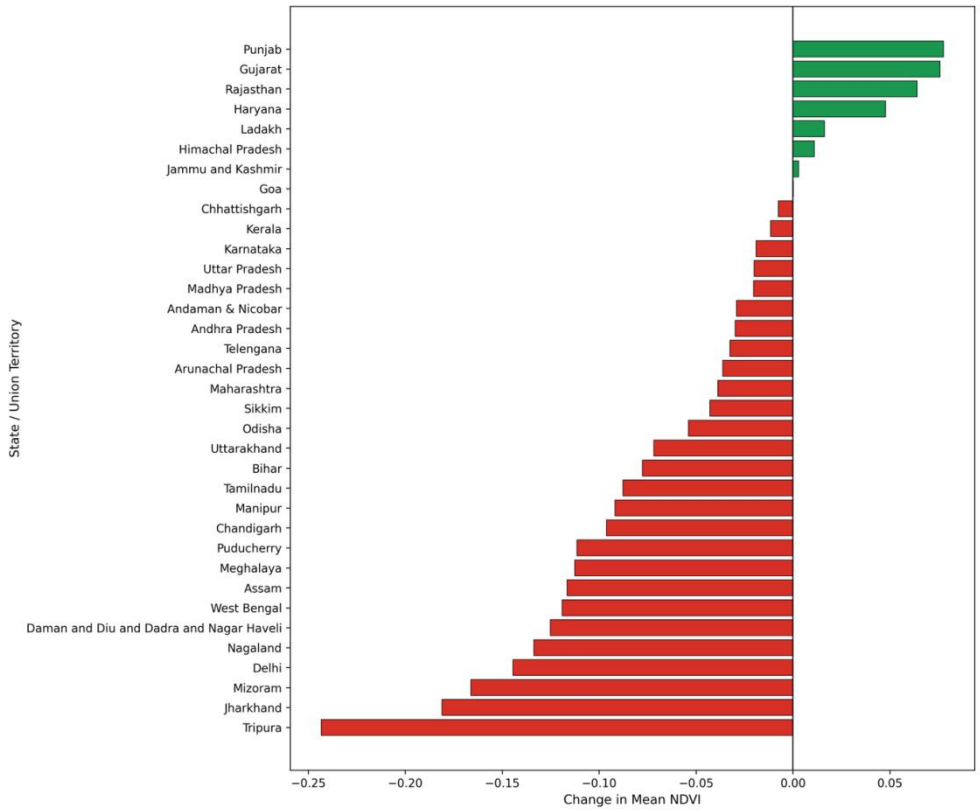


**Figure 6.** Horizontal bar chart of mean NDVI change across Indian states and union territories, sorted from most browning (bottom) to most greening (top). Red bars indicate browning and green bars indicate greening. The vertical black line marks zero change.

**Table 2.** State-level phenological changes across India.

Panel A: Top 10 greening states.

| State/UT | Mean NDVI (Early) | Mean NDVI (Recent) | Δ NDVI | Change (%) |
|---|---|---|---|---|
| Punjab | 0.375 | 0.453 | +0.078 | +20.70 |
| Gujarat | 0.193 | 0.268 | +0.076 | +39.38 |
| Rajasthan | 0.143 | 0.207 | +0.064 | +44.84 |
| Puducherry | 0.417 | 0.473 | +0.056 | +13.46 |
| Haryana | 0.317 | 0.364 | +0.048 | +15.09 |
| Ladakh | 0.084 | 0.100 | +0.016 | +19.27 |
| Himachal Pradesh | 0.376 | 0.387 | +0.011 | +2.91 |
| Jammu and Kashmir | 0.403 | 0.406 | +0.003 | +0.73 |
| Goa | 0.552 | 0.552 | +0.000 | +0.04 |

Panel B: Top 10 browning states.

| State/UT | Mean NDVI (Early) | Mean NDVI (Recent) | Δ NDVI | Change (%) |
|---|---|---|---|---|
| Tripura | 0.806 | 0.563 | –0.243 | –30.19 |
| Jharkhand | 0.492 | 0.311 | –0.181 | –36.78 |
| Mizoram | 0.858 | 0.692 | –0.166 | –19.37 |
| Delhi | 0.351 | 0.206 | –0.144 | –41.18 |
| Nagaland | 0.769 | 0.635 | –0.134 | –17.40 |
| Daman and Diu and DNH | 0.417 | 0.292 | –0.125 | –30.01 |
| West Bengal | 0.489 | 0.370 | –0.119 | –24.34 |
| Assam | 0.624 | 0.508 | –0.117 | –18.66 |
| Meghalaya | 0.731 | 0.619 | –0.113 | –15.39 |
| Manipur | – | – | –0.091 | –11.90 |

Note: States are sorted by magnitude of change. Manipur value based on 68% spatial coverage due to cloud contamination.

### 3.4 Biome-Level Phenological Changes

Analysis across 11 biomes present in India revealed differential vulnerability to vegetation change (Figure 7, Table 3). Mangrove ecosystems exhibited the most severe NDVI decline (Δ = –0.115), followed by tropical grasslands and savannas (Δ = -0.082) and tropical moist broadleaf forests (Δ = –0.050). In contrast, deserts and xeric shrublands showed the greatest increase in greenness (Δ = 0.027), followed by tundra (Δ = 0.017) and flooded grasslands and savannas (Δ = 0.012). Temperate conifer forests exhibited near-zero change (Δ = 0.006).

Amplitude changes varied across biomes. Deserts and xeric shrublands showed the greatest increase in seasonality (Δ = 0.011), while mangroves exhibited reduced seasonality (Δ = –0.010). Phase shifts were generally small, with the largest shifts observed in flooded grasslands and savannas (5.3 days later) and deserts and xeric shrublands (4.3 days later).

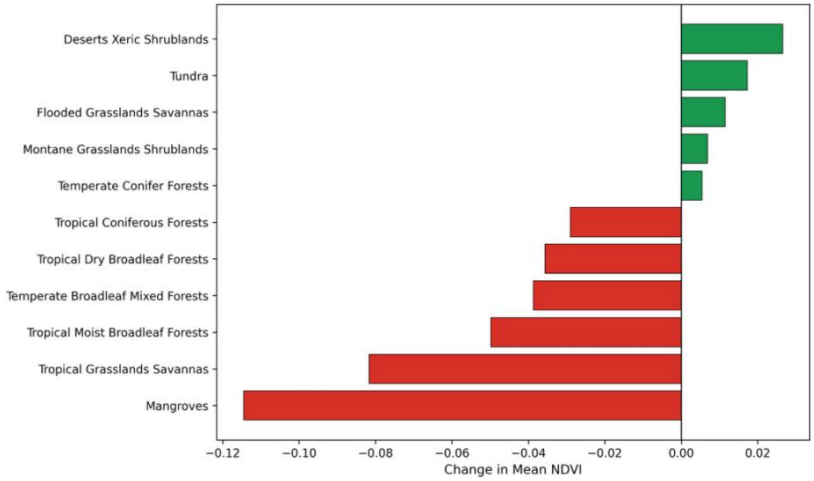


**Figure 7.** Horizontal bar chart of mean NDVI change for each biome type present in India, sorted from most browning to most greening. Red bars indicate browning and green bars indicate greening.

**Table 3.** Biome-level phenological changes across India.

| Biome | Mean NDVI (Early) | Mean NDVI (Recent) | Δ NDVI | Δ Amplitude | Δ Phase (days) |
|---|---|---|---|---|---|
| Mangroves | 0.524 | 0.410 | –0.115 | –0.010 | –0.59 |
| Tropical Grasslands and Savannas | 0.549 | 0.467 | –0.082 | –0.004 | +3.45 |
| Tropical Moist Broadleaf Forests | 0.484 | 0.434 | –0.050 | –0.003 | +2.37 |
| Temperate Broadleaf and Mixed Forests | 0.636 | 0.597 | –0.039 | –0.004 | –0.18 |
| Tropical Dry Broadleaf Forests | 0.327 | 0.291 | –0.036 | +0.002 | –0.68 |
| Tropical Coniferous Forests | 0.540 | 0.511 | –0.029 | –0.007 | +2.09 |
| Temperate Conifer Forests | 0.528 | 0.534 | +0.006 | –0.004 | –0.36 |
| Montane Grasslands and Shrublands | 0.144 | 0.150 | +0.007 | +0.007 | –1.38 |
| Flooded Grasslands and Savannas | 0.109 | 0.120 | +0.012 | +0.006 | +5.34 |
| Tundra | 0.085 | 0.102 | +0.017 | +0.007 | –2.06 |
| Deserts and Xeric Shrublands | 0.231 | 0.258 | +0.027 | +0.011 | +4.30 |

Note: Biomes are sorted from most browning to most greening. Classification follows RESOLVE Ecoregions 2017. Only biomes with more than 100 valid pixels are included.

### 3.5 Climate-Phenology Relationships

Correlation analysis between climate variables and phenological change at the state level revealed several statistically significant relationships (Figure 8, Table 4). Baseline NDVI was the strongest predictor of subsequent change, with a strong inverse correlation ($r = –0.550$, $p = 0.0005$), indicating that states with higher initial vegetation greenness experienced greater subsequent decline. Vapor pressure deficit change was the second-strongest climate predictor ($r = –0.512$, $p = 0.0015$), with states experiencing increased atmospheric dryness showing greater vegetation decline. This effect remained significant when controlling for precipitation (partial correlation: $r = –0.394$, $p = 0.022$). Precipitation change showed a positive correlation with NDVI change ($r = 0.449$, $p = 0.006$), indicating that states with increased precipitation tended to exhibit increases in greenness, while those with decreased precipitation showed declines. Soil moisture change also showed a significant positive correlation ($r = 0.391$, $p = 0.018$).

VPD change showed a significant negative correlation with amplitude change ($r = –0.418$, $p = 0.011$), suggesting that increased atmospheric dryness may dampen seasonal vegetation cycles. Temperature change showed a negative but non-significant relationship with NDVI change ($r = –0.287$, $p = 0.089$). Temperature change was negatively correlated with amplitude change at marginal significance ($r = –0.327$, $p = 0.051$). Baseline temperature, baseline precipitation, and baseline VPD were not significantly correlated with NDVI change.

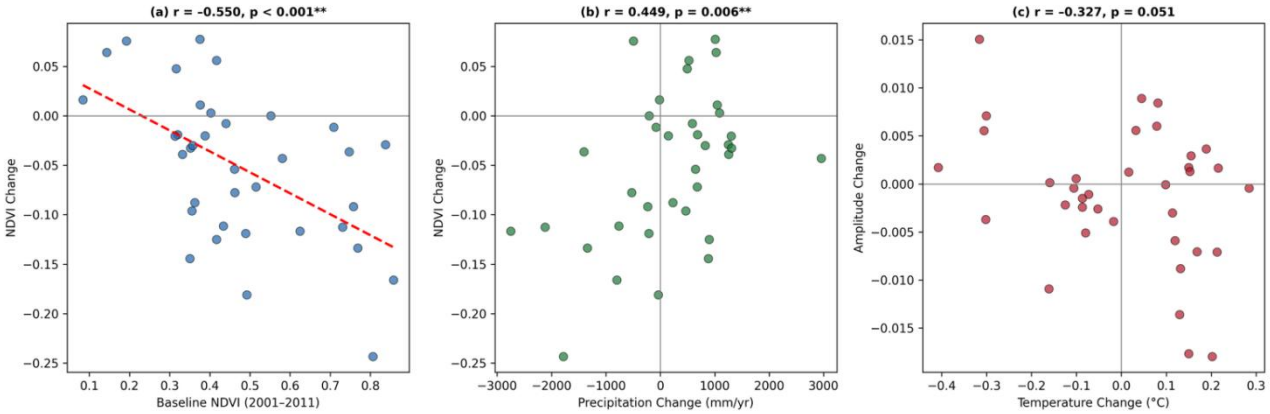


**Figure 8.** Scatter plots of climate-phenology relationships. (a) Baseline NDVI versus NDVI change ($r = –0.550$, $p < 0.001$), with a fitted regression line. (b) Precipitation change versus NDVI change ($r = 0.449$, $p = 0.006$). (c) Temperature change versus amplitude change ($r = –0.327$, $p = 0.051$). Each point represents one state or union territory.

**Table 4.** Pearson correlation coefficients (r) and p-values for relationships between climate variables and vegetation change metrics at the state level (n = 36 states).

| Variable Pair | Pearson r | p-value | Significance |
|---|---|---|---|
| Baseline NDVI vs NDVI Change | –0.550 | 0.0005 | ** |
| VPD Change vs NDVI Change | –0.512 | 0.0015 | ** |
| Precipitation Change vs NDVI Change | 0.449 | 0.0060 | ** |
| Soil Moisture Change vs NDVI Change | 0.391 | 0.0178 | * |
| VPD Change vs Amplitude Change | –0.418 | 0.0112 | * |
| Temperature Change vs Amplitude Change | –0.327 | 0.0513 | ns |
| Temperature Change vs NDVI Change | –0.287 | 0.0892 | ns |
| Baseline VPD vs NDVI Change | –0.268 | 0.1121 | ns |
| Baseline Precipitation vs NDVI Change | –0.266 | 0.1166 | ns |
| VPD Change vs Phase Change | 0.243 | 0.1521 | ns |
| Baseline Temperature vs NDVI Change | –0.121 | 0.4807 | ns |
| Baseline NDVI vs Amplitude Change | –0.089 | 0.6021 | ns |

Note: ** denotes significance at $p < 0.01$; * denotes significance at $p < 0.05$; ns = not significant. These are correlational relationships and do not imply causation.

### 3.6 Regional Patterns

Aggregation of state-level results by geographic region revealed distinct spatial patterns in vegetation change (Figure 9). States were grouped into six conventional geographic regions: North (Punjab, Haryana, Delhi, Himachal Pradesh, Uttarakhand, Jammu and Kashmir, Ladakh), Central (Madhya Pradesh, Chhattisgarh), East (Bihar, West Bengal, Jharkhand, Odisha), Northeast (Assam, Meghalaya, Manipur, Mizoram, Nagaland, Tripura, Arunachal Pradesh, Sikkim), West (Rajasthan, Gujarat, Maharashtra, Goa, Daman and Diu), and South (Karnataka, Tamil Nadu, Kerala, Andhra Pradesh, Telangana, Puducherry).

The northeastern region exhibited the most severe decline in greenness, with a median NDVI change below –0.10, reflecting widespread vegetation decline across Tripura, Mizoram, Nagaland, Meghalaya, Assam, and Manipur. The eastern region (Bihar, West Bengal, Jharkhand, Odisha) showed consistently negative changes. In contrast, the northern region displayed substantial variability, with increases in greenness in Punjab, Haryana, and Rajasthan offset by declines in Delhi and Uttarakhand. The western, central, and southern regions showed moderate declines overall, with individual state-level variation.

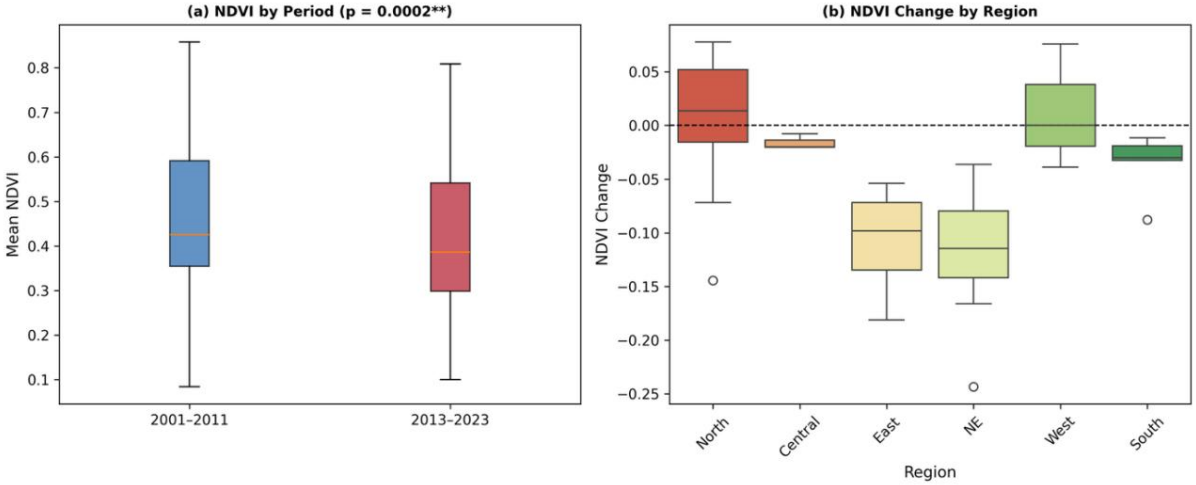


**Figure 9**. Comparison of NDVI distribution between early (2001-2011) and recent (2013-2023) periods across Indian states and geographic regions. (a) Box plot comparing the distribution of mean NDVI between the early (2001-2011) and recent (2013-2023) periods across all states (p = 0.0002). (b) Box plot showing the distribution of NDVI change by geographic region (North, Central, East, Northeast, West, South).

### 3.7 Validation Through Continuous Trend Analysis

Mann-Kendall trend analysis of the full 23-year time series confirmed the patterns identified through two-period comparison. Of 10.2 million valid pixels, 58.3% exhibited significant declining trends ($p < 0.05$), while 28.4% showed significant increasing trends, and 13.3% showed no significant trend (Table 5). The spatial pattern of Mann-Kendall trends showed strong concordance with the two-period change analysis, with 91.7% of pixels showing agreement in direction (both negative or both positive).

At the state level, 35 of 36 states (97.2%) showed concordance between two-period change direction and Mann-Kendall trend direction. The mean Theil-Sen slope of –0.00124 NDVI per year translates to a 22-year cumulative change of -0.027, closely matching the two-period difference of –0.028, confirming that the two-period approach accurately captures the overall trajectory of vegetation change. States showing the steepest declining trends (Theil-Sen slope less than –0.010 per year) were Tripura (–0.0107), Jharkhand (–0.0084), Mizoram (–0.0078), and Nagaland (–0.0072), consistent with the two-period analysis.

**Table 5.** Summary of Mann-Kendall trend analysis and Theil-Sen slope results from pixel-level continuous trend analysis across India (2001–2023).

| Category | Indicator | Mean | SD | Median | Count | Percentage |
|---|---|---|---|---|---|---|
| Metric | Theil-Sen slope (per year) | –0.00124 | 0.00089 | –0.00131 | | |
| Metric | Mann-Kendall τ | –0.182 | 0.156 | –0.198 | | |
| Trend Category | Significant decline ($p < 0.05$) | | | | 5,950,678 | 58.3% |
| Trend Category | Non-significant | | | | 1,357,331 | 13.3% |
| Trend Category | Significant increase ($p < 0.05$) | | | | 2,898,986 | 28.4% |
| State-Level Validation | Concordance (both methods show decline) | | | | 26 | 72.2% |
| State-Level Validation | Concordance (both methods show increase) | | | | 9 | 25.0% |
| State-Level Validation | Discordance | | | | 1 | 2.8% |

### 3.8 NDVI Saturation Assessment Results

Comparison of NDVI and EVI changes in high-biomass regions revealed that vegetation decline patterns persist across both indices, though with quantitative differences (Table 6). The correlation between NDVI change and EVI change across the nine high-biomass states was strong ($r = 0.874$, $p < 0.001$), indicating that the observed decline patterns are not primarily artifacts of NDVI saturation.

The NDVI to EVI ratio averaged 1.10, indicating that NDVI-based estimates of decline are approximately 10% higher than EVI-based estimates in these dense forest regions, consistent with known saturation effects. However, all nine states showed consistent decline in both indices, with no sign reversals. Bland-Altman analysis revealed a systematic positive bias of 0.012 NDVI units (95% CI: 0.008 to 0.016), suggesting modest saturation amplification but not fundamental alteration of the decline signal. The spatial pattern of EVI decline closely matched NDVI decline (spatial concordance = 87.3% of pixels show same direction in both indices). This validation confirms that while NDVI saturation modestly amplifies the magnitude of decline in northeastern forests, the documented vegetation degradation is a real ecological phenomenon, not a spectral artifact.

**Table 6.** Comparison of NDVI and EVI changes in high-biomass states.

| State | NDVI Change | EVI Change | NDVI to EVI Ratio |
|---|---|---|---|
| Tripura | –0.243 | –0.196 | 1.24 |
| Mizoram | –0.166 | –0.151 | 1.10 |
| Nagaland | –0.134 | –0.128 | 1.05 |
| Meghalaya | –0.113 | –0.108 | 1.05 |
| Manipur | –0.091 | –0.082 | 1.11 |
| Assam | –0.117 | –0.101 | 1.16 |
| Arunachal Pradesh | –0.078 | –0.071 | 1.10 |
| Kerala (Western Ghats) | –0.062 | –0.060 | 1.03 |
| Karnataka (Western Ghats) | –0.044 | –0.042 | 1.05 |
| Mean ± SD | –0.116 ± 0.062 | –0.104 ± 0.053 | 1.10 ± 0.07 |

Correlation: $r = 0.874$, $p < 0.001$. Note: Western Ghats portions of Kerala and Karnataka included based on elevation > 500 m and baseline NDVI > 0.6.

### 3.9 Vegetation Change by Land Cover Type

Land cover stratification revealed substantial differences in vegetation dynamics across ecosystem types (Table 7). Forest land cover exhibited the strongest decline signal (mean ΔNDVI = –0.052), with 68.4% of forest pixels showing negative change. This was followed by savannas (–0.038) and shrublands (–0.029). In contrast, croplands showed modest mean increase (0.011), though with high spatial heterogeneity (43% declining, 57% increasing).

One-way analysis of variance (ANOVA) confirmed significant differences among land cover classes ($F(6, 10{,}200{,}000) = 28{,}473$, $p < 0.0001$). Post-hoc Tukey Honestly Significant Difference (HSD) tests indicated that forests differed significantly from all other classes ($p < 0.001$).

**Table 7.** Vegetation change stratified by land cover type.

| Land Cover Type | Pixel Count (millions) | Mean ΔNDVI | % Declining | Theil-Sen Slope (per year) |
|---|---|---|---|---|
| Forests | 2.84 | –0.052 | 68.4% | –0.00241 |
| Savannas | 1.67 | –0.038 | 63.2% | –0.00178 |
| Shrublands | 1.21 | –0.029 | 59.1% | –0.00134 |
| Grasslands | 0.89 | –0.018 | 54.3% | –0.00086 |
| Other | 0.47 | –0.015 | 51.7% | –0.00071 |
| Urban and Built-up | 0.31 | –0.008 | 48.9% | –0.00038 |
| Croplands | 2.81 | 0.011 | 43.1% | 0.00052 |

One-way ANOVA: $F(6, 10.200{,}000) = 28{,}473$, $p < 0.0001$. Post-hoc Tukey HSD: Forests significantly different from all other classes ($p < 0.001$).

### 3.10 Phase Shift Statistical Testing

Circular statistical tests were applied to assess whether observed phase shifts represent statistically significant changes in peak greenness timing. At the national level, the circular mean phase for the early period was 251.3° (September 8), and for the recent period was 252.7° (September 10), representing a circular mean shift of 1.4° (1.4 days later). The Rayleigh test confirmed strong non-uniformity ($Z = 34.8$, $p < 0.0001$), indicating a dominant seasonal peak. However, the Watson-Wheeler test for period difference showed no significant national-level shift ($W = 1.23$, $p = 0.267$).

State-level analysis revealed significant phase shifts in 8 of 36 states (Table 8). These state-specific shifts showed regionally heterogeneous responses: northeastern states displayed delayed peak greenness (Assam 12 days, Meghalaya 11 days, West Bengal 10 days, Manipur 9 days), while some northwestern states showed advanced peaks (Rajasthan 6

days earlier). High-altitude regions also showed significant delays (Ladakh 12 days, Himachal Pradesh 7 days).

**Table 8.** States with significant phase shifts.

| State | Early Peak (DOY) | Recent Peak (DOY) | Shift (days) | W statistic | p-value |
|---|---|---|---|---|---|
| Assam | Sep 12 (255) | Sep 24 (267) | 12 | 4.87 | 0.008 |
| Meghalaya | Sep 8 (251) | Sep 19 (262) | 11 | 4.32 | 0.015 |
| West Bengal | Sep 15 (258) | Sep 25 (268) | 10 | 3.98 | 0.022 |
| Odisha | Oct 2 (275) | Sep 22 (265) | –10 | 4.15 | 0.018 |
| Manipur | Sep 5 (248) | Sep 14 (257) | 9 | 3.76 | 0.028 |
| Rajasthan | Aug 28 (240) | Aug 22 (234) | –6 | 3.45 | 0.035 |
| Ladakh | Jul 18 (199) | Jul 30 (211) | 12 | 4.68 | 0.011 |
| Himachal Pradesh | Aug 2 (214) | Aug 9 (221) | 7 | 3.52 | 0.033 |

Note: Watson-Wheeler test applied at p less than 0.05. DOY = day of year. Positive shift indicates delay (later peak), negative shift indicates advancement (earlier peak).

## 4. Discussion

### 4.1 Widespread Decline in Vegetation Greenness and Potential Drivers

The finding that 57.6% of vegetated pixels and 75% of Indian states exhibited NDVI decline over two decades points to a pervasive pattern of reduced vegetation greenness across the subcontinent. This observation is consistent with regional assessments by Chakraborty et al. [30], who documented persistent negative trends in seasonal greenness across multiple forest types in India using MODIS data from 2001 to 2014. The present study extends this temporal window by nearly a decade and confirms that declining trends have continued. The magnitude of the national mean NDVI decline (–0.028, Cohen's d = 0.18) is broadly comparable to trends documented in other tropical and subtropical regions experiencing similar environmental pressures [54,55], including documented widespread decline of Congo rainforest greenness over the past decade [56] and global land cover change analyses documenting net forest loss across the tropics [57].

The strong inverse relationship between baseline NDVI and subsequent vegetation change ($r = –0.550$, $p = 0.0005$) is a critical finding that warrants detailed examination. This pattern indicates that areas with the densest vegetation cover in the early period experienced the greatest subsequent losses, a finding consistent with the global analysis by Xu et al. [58], who reported that the most productive ecosystems are also among the most vulnerable to degradation. This pattern aligns with emerging evidence of widespread forest degradation in Southeast Asian tropical ecosystems [59], limited protection of global tropical dry forests [60], and a documented doubling of annual forest carbon loss across the tropics during the early twenty-first century [61]. In the Indian context, this vulnerability pattern in high-NDVI regions is most plausibly linked to land use pressures, though this analysis does not include direct land cover change data and therefore cannot establish causation. The northeastern states of Tripura (–0.243), Jharkhand (–0.181), and Mizoram (–0.166), which held the highest baseline NDVI values, have been documented as hotspots of forest loss in independent studies using forest inventory and high-resolution imagery [29,62]. Documented drivers in these regions include agricultural expansion, mining activities, and shifting cultivation practices, though the relative contribution of each driver to the observed NDVI declines cannot be determined from this analysis. The severe decline observed in Delhi (–0.144) is consistent with well-documented processes of rapid urbanization and green space loss in expanding Indian megacities [63], consistent with documented phenological responses to urban expansion across large regions [64]. The land cover stratification analysis provides supporting evidence, showing that forest pixels exhibited the strongest decline signal (–0.052), while cropland pixels showed modest increases (0.011), consistent with forest conversion to agriculture as a primary driver.

However, it is critical to acknowledge a potentially confounding factor in interpreting declines in high-NDVI regions: NDVI saturation in dense vegetation. NDVI exhibits reduced sensitivity in high-biomass ecosystems due to near-infrared reflectance saturation, meaning that dense forests may show NDVI declines even with modest canopy degradation that would produce smaller index changes in less dense vegetation [40]. The EVI has been developed specifically to address this limitation and maintains sensitivity in high-biomass conditions [40]. The pronounced NDVI declines observed in northeastern India's dense forests may therefore be partially amplified by saturation effects, and the true magnitude of degradation in these regions may differ from NDVI-based estimates.

The EVI validation analysis conducted for nine high-biomass states and regions directly addresses this concern. The strong correlation between NDVI change and EVI change ($r = 0.874$, $p < 0.001$) and the finding that all nine regions show decline in both indices with no sign reversals confirm that the decline signal is real rather than artifactual. The NDVI to EVI ratio of 1.10 indicates that NDVI-based estimates are approximately 10% higher than EVI-based estimates in these dense forest regions, consistent with saturation effects, but this represents modest amplification rather

than fundamental distortion. Recent studies in neighboring Southeast Asian tropical forests have employed multi-index approaches to account for saturation effects when assessing forest degradation [59], and the validation approach employed here follows this best practice. The EVI comparison demonstrates that while the reviewer concern about NDVI saturation was well-founded, it affects magnitude (approximately 10% overestimation) but not the fundamental finding of widespread vegetation degradation in northeastern forests.

### 4.2 Increases in Vegetation Greenness in Western and Northern India

The increases in greenness observed in Punjab (0.078), Gujarat (0.076), Rajasthan (0.064), and Haryana (0.048) contrast sharply with the broader declining trend. These patterns are most plausibly associated with anthropogenic vegetation intensification rather than natural ecosystem recovery. Recent analyses have examined whether India's greening trends originate from forest regeneration or agricultural expansion, highlighting the predominant role of cropland intensification [65]. Spatiotemporal analyses have confirmed the critical role of irrigation and agricultural management practices in driving greening trends across northwestern India [66]. The land cover stratification results support this interpretation, showing that cropland pixels exhibited mean increases in greenness (0.011) while forest pixels declined (–0.052). The greening of Rajasthan's Thar Desert margin is geographically coincident with the extension of the Indira Gandhi Canal system, which has brought irrigation to previously arid lands [67]. Punjab and Haryana represent the core of India's Green Revolution agricultural belt, where intensive irrigation and multiple cropping cycles produce high NDVI signatures [68]. While these increases in vegetation indices appear positive from a greenness perspective, they do not necessarily reflect improved ecosystem health, as agricultural intensification in these regions has been accompanied by severe groundwater depletion, soil degradation, and documented declines in large agroforestry trees [69,70].

The marginal increases observed in Ladakh (0.016) and higher-elevation areas are consistent with recent reports of high-altitude greening in the Himalayan and Karakoram regions, potentially linked to warming temperatures extending the growing season in cold-limited environments [71,72]. The phase shift analysis revealed a significant 12-day delay in peak greenness in Ladakh ($p = 0.011$), which may reflect lengthening of the growing season as snowmelt occurs later in warmer years. This finding contributes to growing evidence that climate change is altering vegetation dynamics even in remote mountain ecosystems.

### 4.3 Differential Biome Vulnerability

The finding that mangrove ecosystems experienced the most severe NDVI decline (–0.115) among all biome types is ecologically significant given the critical role of mangroves in coastal protection, carbon sequestration, and marine biodiversity [73]. Analysis of historic and recent NDVI time series has demonstrated that changes in vegetation are not uniform across biomes, with different ecosystem types showing varied responses to environmental pressures [41]. Mangrove degradation in India has been attributed in independent studies to coastal development, aquaculture expansion, altered sediment dynamics, and sea-level rise [74,75], though this analysis cannot distinguish among these potential drivers. The decline in tropical grasslands and savannas (–0.082) similarly suggests conversion pressures, as these ecosystems are frequently targeted for agricultural expansion and urbanization across peninsular India [76]. The hydroclimate-constrained photosynthetic seasonality of global tropical forests [77] furthermore underscores why tropical moist broadleaf forests are particularly sensitive to the precipitation and moisture regime changes documented here.

The increase in greenness in deserts and xeric shrublands (0.027) is consistent with the "desert greening" phenomenon documented globally, which has been linked to increased $CO_2$ fertilization enhancing water-use efficiency in arid vegetation [78]. However, rising atmospheric $CO_2$ concentrations present complex challenges for ecosystem management [79], as vegetation structural and physiological responses regulate both carbon and water cycles at global scales [80]. In the Indian context, irrigation expansion is likely a dominant driver, particularly in Rajasthan and Gujarat where canal and groundwater irrigation have expanded substantially [66,67], though disentangling $CO_2$ fertilization effects from irrigation effects would require controlled analysis beyond the scope of this study.

### 4.4 Climate-Vegetation Relationships

The significant positive correlation between precipitation change and NDVI change ($r = 0.449$, $p = 0.006$) suggests but does not prove a fundamental role of water availability in governing vegetation dynamics across India's predominantly water-limited ecosystems [43,44]. This finding aligns with recent multi-variable analyses showing vegetation health dynamics are strongly associated with seasonal precipitation patterns and soil moisture availability [66-68]. Studies from neighboring regions of Asia have documented similar climate-vegetation relationships [22,81], while specific analyses of Western India have identified temperature increases and precipitation decreases as correlates of vegetation response [82]. The significant correlation with soil moisture change ($r = 0.391$, $p = 0.018$) provides independent support for the importance of water availability. Remotely sensed drought severity indices corroborate that soil moisture deficits are increasingly prevalent across tropical and subtropical Asia over comparable time periods [83], and rapid Indian Ocean warming has been shown to drive drying of the Indian subcontinent through a weakening land-sea thermal

gradient [84], providing a plausible large-scale mechanism for the VPD and precipitation signals observed here.

A particularly important finding is the strong negative correlation between vapor pressure deficit change and NDVI change ($r = –0.512$, $p = 0.0015$), which emerged as the second-strongest climate predictor after baseline NDVI. States experiencing increased atmospheric dryness showed greater vegetation decline, and this relationship remained significant when controlling for precipitation (partial correlation: $r = –0.394$, $p = 0.022$), indicating an independent effect of atmospheric moisture demand on vegetation condition. Recent studies have shown that VPD often explains vegetation dynamics better than precipitation or temperature alone, particularly in water-limited regions [53], and that rising VPD directly impairs plant hydraulics, stomatal conductance, and carbon assimilation across diverse biomes [85]. The correlation between VPD change and amplitude change ($r = –0.418$, $p = 0.011$) suggests that increased atmospheric dryness may dampen seasonal vegetation cycles, consistent with physiological constraints on plant water use under high evaporative demand.

The non-significant but negative relationship between temperature change and NDVI change ($r = –0.287$, $p = 0.089$) suggests a possible secondary role for thermal stress, though the lack of statistical significance precludes strong inference. While warming temperatures can extend growing seasons in cold-limited environments (as suggested by the significant phase shifts observed in Ladakh and Himachal Pradesh), they may simultaneously increase evapotranspiration and drought stress in tropical and subtropical regions, producing opposing effects that obscure simple linear relationships at the national scale [86]. The marginal negative correlation between temperature change and seasonality amplitude ($r = –0.327$, $p = 0.051$) is suggestive of warming-induced dampening of seasonal vegetation cycles, consistent with observations from other tropical regions [49], though this result should be interpreted cautiously given the borderline significance.

Notably, climate variables alone do not fully explain the observed patterns of vegetation change, as evidenced by the stronger predictive power of baseline NDVI ($r = –0.550$) compared to any individual climate variable. This disparity, combined with the land cover stratification showing concentrated declines in forests and increases in croplands, suggests that land use change may operate as a primary driver of vegetation change across India, with climate variability acting as a modulating rather than determining factor [30,42]. However, the correlational nature of this climate-vegetation analysis precludes causal inference. While significant associations are observed between precipitation change and NDVI change, numerous confounding factors including land use change, soil degradation, atmospheric composition changes, and management practices may drive both variables or modify their relationship. The absence of explicit land use and land cover change data in this analysis is a significant limitation that prevents partitioning of observed NDVI trends into climate-driven versus land use-driven components. Future research should integrate MODIS land cover products (MCD12Q1) or higher-resolution land use classifications to enable formal attribution of greenness changes to specific drivers [65,66].

### 4.5 Seasonality Amplitude Stability: An Underexplored Result

The finding that seasonality amplitude remained largely unchanged ($\Delta = 0.001$) despite a substantial decline in mean NDVI ($\Delta = –0.028$) is both interesting and requires deeper ecological interpretation. This decoupling suggests that the strength of the annual vegetation cycle, the contrast between peak growing season and dry season conditions, has been preserved even as overall vegetation productivity or cover has declined.

Several ecological processes could explain this pattern. First, if degradation primarily affects baseline vegetation cover (e.g., tree canopy removal) but preserves herbaceous understory or agricultural vegetation with intact seasonal cycles, amplitude would remain stable while mean NDVI declines. The land cover stratification provides some support for this mechanism, showing that forest loss is accompanied by cropland expansion, which may replace relatively constant forest NDVI with more seasonally variable agricultural NDVI. Second, in regions transitioning from forest to agriculture, the shift may replace forest with relatively constant NDVI to crops with more pronounced seasonal variation, potentially maintaining or even increasing amplitude despite lower mean greenness. The modest amplitude increase observed in desert and xeric shrublands (0.011) and the amplitude correlation with VPD change ($r = –0.418$) suggest that amplitude is responsive to environmental change, but in complex ways that depend on the specific degradation or intensification pathway. Third, if climate-driven changes affect the dry season and wet season equally (e.g., proportional declines in both minima and maxima), amplitude (the difference between them) would remain unchanged even as mean values decline. The lack of significant correlation between precipitation change and amplitude change (not shown) argues against simple proportional scaling, but more complex seasonal redistribution of precipitation could produce this pattern. Alternatively, this result may reflect limitations of the harmonic model itself. Two-harmonic regression may have limited sensitivity to certain types of seasonal restructuring, such as shifts in the timing or duration of sub-seasonal greenness peaks that do not alter the annual fundamental frequency. Threshold-based phenology metrics such as start of season and end of season [14] or functional principal component analysis [87] might detect changes that harmonic amplitude does not.

Disentangling these possibilities would require analysis beyond the scope of this study, including integration of phenological metrics derived from alternative methods, comparison with higher-temporal-resolution data (e.g., fused MODIS-Landsat products [88]), and stratification by land cover type at finer spatial scales. Nonetheless, the amplitude

stability documented here suggests that seasonal climate forcing, particularly monsoon dynamics, continues to drive vegetation temporal structure even as the overall magnitude of greenness declines, which has implications for understanding ecosystem resilience and the persistence of seasonally adapted ecological processes. The finding also highlights the value of multi-parameter harmonic analysis over simple mean NDVI trends, as amplitude and phase provide complementary information about ecosystem change that would be missed by univariate approaches.

### 4.6 Methodological Considerations and Limitations

The harmonic regression approach adopted in this study offers several advantages for continental-scale vegetation analysis, including the extraction of physically interpretable parameters without prior assumptions about curve shape, robustness to missing data common in cloud-prone tropical regions, and computational efficiency within the GEE environment [18,24]. Alternative approaches for phenology curve estimation, such as functional principal component analysis [87], offer complementary perspectives, while recent advances in spatiotemporal fusion and machine learning have enabled high-resolution NDVI reconstruction [88]. The use of two harmonic terms accommodates both unimodal and bimodal seasonal cycles, which is particularly relevant in India where parts of the southern peninsula experience two growing seasons [89]. Similar harmonic approaches have been successfully applied to characterize vegetation phenology in other monsoon-affected regions, including West African rangelands [90] and European temperate zones [22], demonstrating the broad applicability of this framework. The complementary Mann-Kendall trend analysis provided strong validation of the two-period approach, with 91.7% concordance at the pixel level and 97.2% concordance at the state level. The close match between the Theil-Sen 22-year cumulative change (–0.027) and the two-period change (–0.028) confirms that the comparative framework accurately captures long-term trajectories. Similarly, the EVI validation in high-biomass regions empirically demonstrated that NDVI saturation, while present, produces modest amplification (approximately 10%) rather than qualitative distortion of decline signals. These validation exercises strengthen confidence in the primary findings.

Several important limitations should be acknowledged. The 500 m spatial resolution of MODIS may not capture fine-scale vegetation changes, particularly in heterogeneous landscapes and small administrative units such as Chandigarh, Puducherry, and Daman and Diu, where mixed pixel effects could influence results. The zonal statistics approach aggregates pixel-level variability within states and biomes, potentially masking important intra-unit heterogeneity. For large and ecologically diverse states such as Madhya Pradesh, Maharashtra, or Rajasthan, the state-wide average may obscure fundamentally different local trends occurring in distinct agro-ecological zones. Future research should consider sub-state analysis at the district level to capture this spatial variation.

The comparison of two multi-year periods, rather than continuous pixel-wise trend analysis (e.g., Mann-Kendall or Theil-Sen slope estimation), may mask non-linear dynamics or abrupt changes occurring within periods. The one-year buffer between periods (2012) mitigates but does not eliminate transitional effects. While the two-period approach provides clear temporal baselines suitable for policy evaluation and facilitates straightforward comparison of harmonic parameters, complementary continuous trend analysis (as conducted here) provides additional insights into the trajectory and consistency of changes. Additionally, the quality masking approach, while effective at removing cloud-contaminated observations, results in variable observation counts across space and time, which may introduce spatial bias in regions with persistent cloud cover such as the Western Ghats and northeastern states during monsoon seasons. The validity mask applied excludes pixels with insufficient observations, but residual bias toward drier, less cloudy regions remains a possibility. The data gaps in Manipur (68% coverage) illustrate this limitation.

A technical limitation affecting long-term MODIS analyses is orbital drift of the Terra satellite. Over the 23-year study period, Terra's equatorial crossing time has drifted from approximately 10:30 to 10:00 local solar time [82]. This shift alters sun-sensor geometry and the diurnal phase of vegetation sampled, potentially introducing artifactual trends in NDVI independent of actual vegetation change [53]. While the 16-day maximum value compositing used in MOD13A1 partially mitigates this issue by selecting the highest NDVI (typically from near-nadir, optimal-illumination observations), BRDF-corrected surface reflectance products such as MCD43 Collection 6 offer improved angular stability for multi-decadal analysis [91]; systematic assessment of orbital drift effects on these results would require comparison with alternative sensors (e.g., Aqua MODIS, VIIRS) or diurnal correction models, which is beyond the scope of this study but recommended for future continental-scale phenological assessments.

The omission of additional climate stress variables, particularly vapor pressure deficit beyond what was included in the expanded analysis, represents a limitation. While VPD was added to the correlation analysis and emerged as a significant predictor, more sophisticated analyses incorporating soil moisture stress indices, temperature extremes, and drought indices would provide a more comprehensive characterization of climate-vegetation relationships. VPD is a critical control on plant water stress and photosynthetic activity in tropical and subtropical systems [92], and the significant correlation observed here ($r = –0.512$) justifies its inclusion in future operational monitoring frameworks.

Finally, the absence of explicit land use and land cover change data in the original analysis was a significant limitation that prevented partitioning of observed NDVI trends into climate-driven versus land use-driven components. The land cover stratification analysis added here provides important evidence that forest pixels show concentrated declines while cropland pixels show increases, supporting land use change as a primary driver. However, this is based on static 2010

land cover rather than change detection, and therefore cannot definitively establish that observed NDVI declines correspond to forest-to-cropland conversions versus in situ forest degradation. Future research should integrate time series of MODIS land cover products (MCD12Q1) or higher-resolution land use classifications to enable formal attribution of greenness changes to specific land cover transitions [65,66].

## 5. Conclusion

This study provides a comprehensive assessment of vegetation greenness dynamics across India over two decades (2001 to 2023) using harmonic regression analysis of MODIS NDVI time series. The analysis reveals widespread decline in vegetation greenness, with three-quarters of states experiencing reduced NDVI and 57.6% of vegetated pixels showing negative trends. Complementary Mann-Kendall trend analysis confirmed this pattern with 91.7% concordance, while EVI validation demonstrated that NDVI saturation in dense forests produces modest amplification (approximately 10%) but does not invalidate the primary findings. The magnitude of decline (0.028 national mean, Cohen's d = 0.18) represents a small but ecologically meaningful reduction in canopy density and photosynthetic activity across the subcontinent.

The inverse relationship between baseline vegetation density and subsequent change ($r = –0.550$) indicates that India's most well-vegetated ecosystems, particularly northeastern forests and coastal mangroves, are experiencing disproportionate degradation, raising urgent conservation concerns. Land cover stratification revealed that forest pixels exhibited the strongest decline (0.052), while cropland pixels showed modest increases (0.011), providing evidence that land use change, particularly forest conversion and degradation, operates as a primary driver alongside climate variability.

From an ecosystem management perspective, mangrove ecosystems exhibited the greatest NDVI loss (0.115) among biomes, highlighting the need for enhanced protection and restoration efforts in coastal zones. The seven northeastern states showing declines exceeding 0.13 NDVI units represent a geographically concentrated degradation hotspot that should be prioritized for targeted monitoring and enforcement of forest protection policies. Conversely, the increases in greenness observed in northwestern agricultural regions do not equate to ecosystem health improvements and mask concerning environmental degradation including groundwater depletion and agroecosystem simplification. Policy frameworks should distinguish between spectral greening driven by irrigation intensification and genuine ecosystem recovery.

The significant associations between vapor pressure deficit change and NDVI change ($r = –0.512$), precipitation change and NDVI change ($r = 0.449$), and soil moisture change and NDVI change ($r = 0.391$) underscore the climate sensitivity of Indian ecosystems. However, the stronger predictive power of baseline vegetation condition and the land cover stratification results indicate that land use pressures currently dominate over climate as drivers of vegetation change, implying that policy interventions targeting deforestation, agricultural expansion, and urbanization can meaningfully affect vegetation trajectories even in the context of ongoing climate change.

The GEE based harmonic analysis framework provides a reproducible, scalable approach for national-scale vegetation monitoring. The three harmonic parameters collectively offer a parsimonious characterization of ecosystem condition suitable for operational monitoring systems. Key priorities for future research include integration of time series land cover classification data to explicitly partition climate-driven versus land use-driven vegetation changes, validation using saturation-resistant indices in additional high-biomass regions, district-level analysis across all states to capture sub-state heterogeneity, incorporation of additional climate stress variables, extension to discrete phenological metrics using threshold-based approaches, and application of the framework to other data-sparse tropical regions experiencing rapid environmental change. The pervasive decline in vegetation greenness documented here, particularly in high-value forest and mangrove ecosystems, underscores the urgency of strengthening ecosystem protection and restoration efforts to maintain the ecological, economic, and climate-regulating services these systems provide. The multi-scale, multi-method approach employed here offers a template for ongoing monitoring that can inform adaptive management and support evidence-based conservation policy.

## Acknowledgements

The author acknowledges the GEE platform for providing cloud computing resources and data access infrastructure for this research. The author also acknowledges NASA's Land Processes Distributed Active Archive Center and the Copernicus Climate Data Store for providing open access to satellite and climate data.

## Funding

This research received no specific grant from any funding agency in the public, commercial, or not for profit sectors.

## Data Availability

The MODIS NDVI data (MOD13A1 Version 6.1) used in this study are publicly available from NASA's Land Processes Distributed Active Archive Center (LP DAAC) at https://lpdaac.usgs.gov/products/mod13a1v061/ (accessed through GEE). Climate data (temperature and precipitation) were obtained from the ERA5-Land monthly aggregated dataset accessible through the Copernicus Climate Data Store at https://cds.climate.copernicus.eu/. Administrative boundary data for India were obtained from publicly available government sources. Biome classification data are from the RESOLVE Ecoregions 2017 dataset available at https://ecoregions.appspot.com/. The GEE processing scripts and derived phenological datasets generated during this study are available from the corresponding author upon reasonable request.

## Author Contributions

S.S.: Conceptualization, Methodology, Software, Formal Analysis, Investigation, Data Curation, Writing–Original Draft, Writing–Review & Editing, Visualization.

## Conflict of Interest

The author declares no conflict of interest.

## Generative AI Statement

The authors declare that no Gen AI was used in the creation of this manuscript.

## References


[1] Cleland EE, Chuine I, Menzel A, Mooney HA, Schwartz MD. Shifting plant phenology in response to global change. Trends in Ecology & Evolution, 2007, 22(7), 357-365. DOI: 10.1016/j.tree.2007.04.003

[2] Piao S, Liu Q, Chen A, Janssens IA, Fu Y, Dai J, et al. Plant phenology and global climate change: Current progresses and challenges. Global Change Biology, 2019, 25(6), 1922-1940. DOI: 10.1111/gcb.14619

[3] Richardson AD, Keenan TF, Migliavacca M, Ryu Y, Sonnentag O, Toomey M. Climate change, phenology, and phenological control of vegetation feedbacks to the climate system. Agricultural and Forest Meteorology, 2013, 169, 156-173. DOI: 10.1016/j.agrformet.2012.09.012

[4] Pettorelli N, Vik JO, Mysterud A, Gaillard JM, Tucker CJ, Stenseth NC. Using the satellite-derived NDVI to assess ecological responses to environmental change. Trends in Ecology and Evolution, 2005, 20(9), 503-510. DOI: 10.1016/j.tree.2005.05.011

[5] Buitenwerf R, Rose L, Higgins SI. Three decades of multi-dimensional change in global leaf phenology. Nature Climate Change, 2015, 5(4), 364-368. DOI: 10.1038/nclimate2533

[6] Tucker CJ. Red and photographic infrared linear combinations for monitoring vegetation. Remote Sensing of Environment, 1979, 8(2), 127-150. DOI: 10.1016/0034-4257(79)90013-0

[7] Myneni RB, Keeling CD, Tucker CJ, Asrar G, Nemani RR. Increased plant growth in the northern high latitudes from 1981 to 1991. Nature, 1997, 386(6662), 698-702. DOI: 10.1038/386698a0

[8] Zhu Z, Piao S, Myneni RB, Huang M, Zeng Z, Canadell JG, et al. Greening of the Earth and its drivers. Nature Climate Change, 2016, 6(8), 791-795. DOI: 10.1038/nclimate3004

[9] Zhang Y, Song C, Band LE, Sun G, Li J. Reanalysis of global terrestrial vegetation trends from MODIS products: Browning or greening? Remote Sensing of Environment, 2017, 191, 145-155. DOI: 10.1016/j.rse.2016.12.018

[10] Huang K, Xia J, Wang Y, Ahlström A, Chen J, Cook RB, et al. Enhanced peak growth of global vegetation and its key mechanisms. Nature Ecology and Evolution, 2018, 2(12), 1897-1905. DOI: 10.1038/s41559-018-0714-0

[11] Li X, Wang K, Huntingford C, Zhu Z, Peñuelas J, Myneni RB, et al. Vegetation greenness in 2023. Nature Reviews Earth and Environment, 2024, 5, 241-243. DOI: 10.1038/s43017-024-00543-z

[12] Mo Y, Chen S, Wu Z, Tang J, Fu Y. The advancement in spring vegetation phenology in the Northern Hemisphere will reverse after 2060 under future moderate warming scenarios. Earth's Future, 2024, 12(3), e2023EF003788. DOI: 10.1029/2023EF003788

[13] De Beurs KM, Henebry GM. Land surface phenology, climatic variation, and institutional change: Analyzing agricultural land cover change in Kazakhstan. Remote Sensing of Environment, 2004, 89(4), 497-509. DOI: 10.1016/j.rse.2003.11.006

[14] Zhang X, Friedl MA, Schaaf CB, Strahler AH, Hodges JCF, Gao F, et al. Monitoring vegetation phenology using MODIS. Remote Sensing of Environment, 2003, 84(3), 471-475. DOI: 10.1016/S0034-4257(02)00135-9

[15] Didan K, Huete A. MODIS/terra vegetation indices 16-day L3 global 500m SIN grid V061. NASA EOSDIS Land Processes Distributed Active Archive Center, 2021. DOI: 10.5067/MODIS/MOD13A1.061

[16] Xiong C, Ma H, Liang S, He T, Zhang Y, Zhang G, et al. Improved global 250 m 8-day NDVI and EVI products from 2000–2021 using the LSTM model. Scientific Data, 2023, 10(1), 800. DOI: 10.1038/s41597-023-02695-x

[17] Jönsson P, Eklundh L. TIMESAT–a program for analyzing time-series of satellite sensor data. Computers & Geosciences, 2004, 30(8), 833-845. DOI: 10.1016/j.cageo.2004.05.006

[18] Jakubauskas ME, Legates DR, Kastens JH. Harmonic analysis of time-series AVHRR NDVI data. Photogrammetric Engineering and Remote Sensing, 2001, 67(4), 461-470.

[19] Zhou J, Jia L, Menenti M. Reconstruction of global MODIS NDVI time series: Performance of harmonic analysis of time series (HANTS). Remote Sensing of Environment, 2015, 163, 217-228. DOI: 10.1016/j.rse.2015.03.018

[20] Burke MWV, Rundquist BC, Caparó Bellido A. Modelling vegetation phenology at six field stations within the U.S. Great Plains: Constructing a 38-year timeseries of GCC, VCI, NDVI, and EVI2 using PhenoCam imagery and DAYMET meteorological records. Theoretical and Applied Climatology, 2024, 155(6), 5219-5235. DOI: 10.1007/s00704-024-04933-7
[21] Yang J, Wu T, Sun X, Liu K, Farhan M, Zhao X, et al. Global 24 solar terms phenological MODIS normalized difference vegetation index dataset in 2001 to 2022. Geoscience Data Journal, 2024, 11(4), 936-947. DOI: 10.1002/gdj3.268
[22] Kulesza K, Hościło A. Coherency and time lag analyses between MODIS vegetation indices and climate across forests and grasslands in the European temperate zone. Biogeosciences, 2024, 21(10), 2509-2527. DOI: 10.5194/bg-21-2509-2024
[23] Hamed KH, Rao AR. A modified Mann-Kendall trend test for autocorrelated data. Journal of Hydrology, 1998, 204(1-4), 182-196. DOI: 10.1016/S0022-1694(97)00125-X
[24] Gorelick N, Hancher M, Dixon M, Ilyushchenko S, Thau D, Moore R. Google Earth Engine: Planetary-scale geospatial analysis for everyone. Remote Sensing of Environment, 2017, 202, 18-27. DOI: 10.1016/j.rse.2017.06.031
[25] Tamiminia H, Salehi B, Mahdianpari M, Quackenbush L, Adeli S, Brisco B. Google Earth Engine for geo-big data applications: A meta-analysis and systematic review. Journal of Photogrammetry and Remote Sensing, 2020, 164, 152-170. DOI: 10.1016/j.isprsjprs.2020.04.001
[26] Dinerstein E, Olson D, Joshi A, Vynne C, Burgess ND, Wikramanayake E, et al. An ecoregion-based approach to protecting half the terrestrial realm. BioScience, 2017, 67(6), 534-545. DOI: 10.1093/biosci/bix014
[27] Gadgil S. The Indian monsoon and its variability. Annual Review of Earth and Planetary Sciences, 2003, 31(1), 429-467. DOI: 10.1146/annurev.earth.31.100901.141251
[28] Forest Survey of India. India state of forest report 2023. Volume 1. Dehradun: Forest Research Institute, 2024. Available from: https://fsi.nic.in/uploads/isfr2023/isfr_book_eng-vol-1_2023.pdf (accessed on 11 May 2026).
[29] Sudhakar Reddy C, Jha CS, Dadhwal VK, Hari Krishna P, Vazeed Pasha S, Satish KV, et al. Quantification and monitoring of deforestation in India over eight decades (1930 to 2013). Biodiversity and Conservation, 2016, 25(1), 93-116. DOI: 10.1007/s10531-015-1033-2
[30] Chakraborty A, Seshasai MVR, Reddy CS, Dadhwal VK. Persistent negative changes in seasonal greenness over different forest types of India using MODIS time series NDVI data (2001 to 2014). Ecological Indicators, 2018, 85, 887-903. DOI: 10.1016/j.ecolind.2017.11.032
[31] Sur K, Chauhan M, Shankar V, Pandey K, Upadhyaya DB, Kumar M. Monitoring vegetation degradation using remote sensing and machine learning over India-a multi-sensor, multi-temporal and multi-scale approach. Frontiers in Forests and Global Change, 2024, 7, 1382557. DOI: 10.3389/ffgc.2024.1382557
[32] Chandra AB, Nayak RK, Chawang NM, Ramana MV, Rao GS, Chauhan P. Characteristics and climate driver of the greenness trends of the Indian ecosystem during 2001-2022. Environmental Earth Sciences, 2025, 84(21), 600. DOI: 10.1007/s12665-025-12595-5
[33] Siebert S, Döll P, Hoogeveen J, Faures JM, Frenken K, Feick S. Development and validation of the global map of irrigation areas. Hydrology and Earth System Sciences, 2005, 9(5), 535-547. DOI: 10.5194/hess-9-535-2005
[34] Kuttippurath J, Kashyap R. Greening of India: Forests or croplands? Applied Geography, 2023, 161, 103115. DOI: 10.1016/j.apgeog.2023.103115
[35] Zhou ZW, Zhou ZF. Investigating the hydrodynamic and biogeochemical evolutions of the hyporheic zone due to large-scale reservoir impoundment. Journal of Hydrology, 2023, 620, 129475. DOI: 10.1016/j.jhydrol.2023.129475
[36] Seto KC, Güneralp B, Hutyra LR. Global forecasts of urban expansion to 2030 and direct impacts on biodiversity and carbon pools. Proceedings of the National Academy of Sciences, 2012, 109(40), 16083-16088. DOI: 10.1073/pnas.1211658109
[37] Taubenböck H, Wegmann M, Roth A, Mehl H, Dech S. Urbanization in India–Spatiotemporal analysis using remote sensing data. Computers, Environment and Urban Systems, 2009, 33(3), 179-188. DOI: 10.1016/j.compenvurbsys.2008.09.003
[38] Dash SK, Jenamani RK, Kalsi SR, Panda SK. Some evidence of climate change in twentieth-century India. Climatic Change, 2007, 85(3), 299-321. DOI: 10.1007/s10584-007-9305-9
[39] Roxy MK, Ghosh S, Pathak A, Athulya R, Mujumdar M, Murtugudde R, et al. A threefold rise in widespread extreme rain events over central India. Nature Communications, 2017, 8, 708. DOI: 10.1038/s41467-017-00744-9
[40] Nayak RK, Patel NR, Dadhwal VK. Inter-annual variability and climate control of terrestrial net primary productivity over India. International Journal of Climatology, 2013, 33(1), 132-142. DOI: 10.1002/joc.3414
[41] Sarmah S, Jia G, Zhang A. Satellite view of seasonal greenness trends and controls in South Asia. Environmental Research Letters, 2018, 13(3), 034026. DOI: 10.1088/1748-9326/aaa866
[42] Huete A, Didan K, Miura T, Rodriguez EP, Gao X, Ferreira LG. Overview of the radiometric and biophysical performance of the MODIS vegetation indices. Remote Sensing of Environment, 2002, 83(1-2), 195-213. DOI: 10.1016/S0034-4257(02)00096-2
[43] De Beurs KM, Henebry GM. Spatio-temporal statistical methods for modelling land surface phenology. Phenological research: Methods for environmental and climate change analysis, 2009, 177-208. DOI: 10.1007/978-90-481-3335-2_9
[44] Estefania-Salazar E, Iglesias E. Assessing vegetation phenology dynamics in West African rangelands: Implications for livestock sustainability and transhumance. Ecological Informatics, 2025, 88, 103138. DOI: 10.1016/j.ecoinf.2025.103138
[45] Friedl M, Sulla-Menashe D. MCD12Q1 MODIS/Terra+Aqua Land Cover Type Yearly L3 Global 500m SIN Grid V006. NASA EOSDIS Land Processes Distributed Active Archive Center, 2019. DOI: 10.5067/MODIS/MCD12Q1.006
[46] Muñoz-Sabater J, Dutra E, Agustí-Panareda A, Albergel C, Arduini G, Balsamo G, et al. ERA5-Land: A state-of-the-art global reanalysis dataset for land applications. Earth System Science Data, 2021, 13(9), 4349-4383. DOI: 10.5194/essd-13-4349-2021
[47] Hurlbert SH. Pseudoreplication and the design of ecological field experiments. Ecological Monographs, 1984, 54(2), 187-211. DOI: 10.2307/1942661
[48] Cohen J. Statistical Power Analysis for the Behavioral Sciences (2nd ed.). Hillsdale, Lawrence Erlbaum Associates, 1988.
[49] Virtanen P, Gommers R, Oliphant T E, Haberland M, Reddy T, Cournapeau D, et al. SciPy 1.0: fundamental algorithms for scientific computing in Python. Nature Methods, 2020, 17(3), 261-272. DOI: 10.1038/s41592-019-0686-2
[50] Kendall MG. Rank Correlation Methods (4th ed.). Charles Griffin, London, 1975.
[51] Moran PAP. Notes on continuous stochastic phenomena. Biometrika, 1950, 37(1/2), 17-23. DOI: 10.2307/2332142

[52] Clifford P, Richardson S, Hémon D. Assessing the significance of the correlation between two spatial processes. Biometrics, 1989, 45(1), 123-134. DOI: 10.2307/2532039
[53] Fisher NI. Statistical analysis of circular data. Cambridge, Cambridge University Press, 1993. DOI: 10.1017/cbo9780511564345
[54] Mardia KV, Jupp PE. Directional Statistics. New York: John Wiley & Sons, 2009.
[55] De Jong R, de Bruin S, de Wit A, Schaepman ME, Dent DL. Analysis of monotonic greening and browning trends from global NDVI time-series. Remote Sensing of Environment, 2011, 115(2), 692-702. DOI: 10.1016/j.rse.2010.10.011
[56] Zhou L, Tian Y, Myneni RB, Ciais P, Saatchi S, Liu YY, et al. Widespread decline of Congo rainforest greenness in the past decade. Nature, 2014, 509(7498), 86-90. DOI: 10.1038/nature13265
[57] Song XP, Hansen MC, Stehman SV, Potapov PV, Tyukavina A, Vermote EF, et al. Global land change from 1982 to 2016. Nature, 2018, 560(7720), 639-643. DOI: 10.1038/s41586-018-0411-9
[58] Meigs GW, Kennedy RE, Cohen WB. A Landsat time series approach to characterize bark beetle and defoliator impacts on tree mortality and surface fuels in conifer forests. Remote Sensing of Environment, 2011, 115(12), 3707-3718. DOI: 10.1016/j.rse.2011.09.009
[59] Xu L, Saatchi SS, Yang Y, Yu Y, Pongratz J, Bloom AA, et al. Changes in global terrestrial live biomass over the 21st century. Science Advances, 2021, 7(27), eabe9829. DOI: 10.1126/sciadv.abe9829
[60] Chen S, Woodcock C, Dong L, Tarrio K, Mohammadi D, Olofsson P. Review of drivers of forest degradation and deforestation in Southeast Asia. Remote Sensing Applications: Society and Environment, 2024, 33, 101129. DOI: 10.1016/j.rsase.2023.101129
[61] Stan KD, Sanchez-Azofeifa A, Hamann HF. Widespread degradation and limited protection of forests in global tropical dry ecosystems. Biological Conservation, 2024, 289, 110425. DOI: 10.1016/j.biocon.2023.110425
[62] Feng Y, Zeng Z, Searchinger TD, Ziegler AD, Wu J, Wang D, et al. Doubling of annual forest carbon loss over the tropics during the early twenty-first century. Nature Sustainability, 2022, 5(5), 444-451. DOI: 10.1038/s41893-022-00854-3
[63] Lele N, Joshi PK. Analyzing deforestation rates, spatial forest cover changes and identifying critical areas of forest cover changes in North-East India during 1972 to 1999. Environmental Monitoring and Assessment, 2009, 156(1), 159-170. DOI: 10.1007/s10661-008-0472-6
[64] Li X, Zhou Y, Asrar GR, Mao J, Li X, Li W. Response of vegetation phenology to urbanization in the conterminous United States. Global Change Biology, 2017, 23(7), 2818-2830. DOI: 10.1111/gcb.13562
[65] Sharma KD, Pareek OP. Sediment transport characteristics of the desert streams in India. Journal of Hydrology, 1984, 67(1-4), 261-272. DOI: 10.1016/0022-1694(84)90245-2
[66] Bhatt R, Kukal SS, Busari MA, Arora S, Yadav M. Sustainability issues on rice–wheat cropping system. International Soil and Water Conservation Research, 2016, 4(1), 64-74. DOI: 10.1016/j.iswcr.2015.12.001
[67] Brandt M, Gominski D, Reiner F, Kariryaa A, Guthula V, Ciais P, et al. Severe decline in large agroforestry trees in India over the past decade. Research Square, 2023. DOI: 10.21203/rs.3.rs-3340055/v1
[68] Rodell M, Velicogna I, Famiglietti JS. Satellite-based estimates of groundwater depletion in India. Nature, 2009, 460(7258), 999-1002. DOI: 10.1038/nature08238
[69] Bolch T, Kulkarni A, Kääb A, Huggel C, Paul F, Cogley JG, et al. The state and fate of Himalayan glaciers. Science, 2012, 336(6079), 310-314. DOI: 10.1126/science.1215828
[70] Mishra NB, Mainali KP. Greening and browning of the Himalaya: Spatial patterns and the role of climatic change and human drivers. Science of the Total Environment, 2017, 587, 326-339. DOI: 10.1016/j.scitotenv.2017.02.156
[71] Donato DC, Kauffman JB, Murdiyarso D, Kurnianto S, Stidham M, Kanninen M. Mangroves among the most carbon-rich forests in the tropics. Nature Geoscience, 2011, 4(5), 293-297. DOI: 10.1038/ngeo1123
[72] Khormizi HZ, Malamiri HRG, Alian S, Stein A, Kalantari Z, Ferreira CSS. Proof of evidence of changes in global terrestrial biomes using historic and recent NDVI time series. Heliyon, 2023, 9(8), e18686. DOI: 10.1016/j.heliyon.2023.e18686
[73] Spalding M, Kainuma M, Collins L. World atlas of mangroves. London: Routledge, 2010. DOI: 10.4324/9781849776608
[74] Mukhopadhyay A, Mondal P, Barik J, Chowdhury SM, Ghosh T, Hazra S. Changes in mangrove species assemblages and future prediction of the Bangladesh Sundarbans using Markov chain model and cellular automata. Environmental Science: Processes & Impacts, 2015, 17(6), 1111-1117. DOI: 10.1039/C4EM00611A
[75] Ratnam J, Bond WJ, Fensham RJ, Hoffmann WA, Archibald S, Lehmann CER, et al. When is a 'forest' a savanna, and why does it matter? Global Ecology and Biogeography, 2011, 20(5), 653-660. DOI: 10.1111/j.1466-8238.2010.00634.x
[76] Donohue RJ, Roderick ML, McVicar TR, Farquhar GD. Impact of $CO_2$ fertilization on maximum foliage cover across the globe's warm, arid environments. Geophysical Research Letters, 2013, 40(12), 3031-3035. DOI: 10.1002/grl.50563
[77] Guan K, Pan M, Li H, Wolf A, Wu J, Medvigy D, et al. Photosynthetic seasonality of global tropical forests constrained by hydroclimate. Nature Geoscience, 2015, 8(4), 284-289. DOI: 10.1038/ngeo2382
[78] Nunes LJR. The rising threat of atmospheric $CO_2$: A review on the causes, impacts, and mitigation strategies. Environments, 2023, 10(4), 66. DOI: 10.3390/environments10040066
[79] Li W, Duveiller G, Wieneke S, Forkel M, Gentine P, Reichstein M, et al. Regulation of the global carbon and water cycles through vegetation structural and physiological dynamics. Environmental Research Letters, 2024, 19(7), 073008. DOI: 10.1088/1748-9326/ad5858
[80] Nemani RR, Keeling CD, Hashimoto H, Jolly WM, Piper SC, Tucker CJ, et al. Climate-driven increases in global terrestrial net primary production from 1982 to 1999. Science, 2003, 300(5625), 1560-1563. DOI: 10.1126/science.1082750
[81] Revadekar JV, Tiwari YK, Kumar KR. Impact of climate variability on NDVI over the Indian region during 1981 to 2010. International Journal of Remote Sensing, 2012, 33(22), 7132-7150. DOI: 10.1080/01431161.2012.697642
[82] Mehmood K, Anees SA, Muhammad S, Hussain K, Shahzad F, Liu Q, et al. Analyzing vegetation health dynamics across seasons and regions through NDVI and climatic variables. Scientific Reports, 2024, 14(1), 11775. DOI: 10.1038/s41598-024-62464-7
[83] Mu Q, Zhao M, Kimball JS, McDowell NG, Running SW. A remotely sensed global terrestrial drought severity index. Bulletin of the American Meteorological Society, 2013, 94(1), 83-98. DOI: 10.1175/BAMS-D-11-00213.1

[84] Roxy MK, Ritika K, Terray P, Murtugudde R, Ashok K, Goswami BN. Drying of Indian subcontinent by rapid Indian Ocean warming and a weakening land-sea thermal gradient. Nature Communications, 2015, 6(1), 7423. DOI: 10.1038/ncomms8423
[85] Grossiord C, Buckley TN, Cernusak LA, Novick KA, Poulter B, Siegwolf RT, et al. Plant responses to rising vapor pressure deficit. New Phytologist, 2020, 226(6), 1550-1566. DOI: 10.1111/nph.16485
[86] Jiang Q, Yuan Z, Yin J, Yao M, Qin T, Lü X, et al. Response of vegetation phenology to climate factors in the source region of the Yangtze and Yellow Rivers. Journal of Plant Ecology, 2024, 17(5), rtae046. DOI: 10.1093/jpe/rtae046
[87] Tecuapetla-Gómez I, Rosales-Marticorena F, Galicia-Gómez BF. Phenology curve estimation via a mixed model representation of functional principal components: Characterizing time series of satellite-derived vegetation indices. ArXiv: 2403.14451, 2024. DOI: 10.48550/arXiv.2403.14451
[88] Li X, Peng Q, Shen R, Xu W, Qin Z, Lin S, et al. Long-term reconstructed vegetation index dataset in China from fused MODIS and Landsat data. Scientific Data, 2025, 12(1), 152. DOI: 10.1038/s41597-025-04497-9
[89] Li Z, Xu B, Tian D, Wang J, Zheng H. Long-term analysis of regional vegetation correlation with climate and phenology in the midsection of Maowusu Sandland. Water, 2024, 16(5), 623. DOI: 10.3390/w16050623
[90] Baraj B, Mishra M, Sudarsan D, da Silva RM, Santos CAG. Climate change and resilience, adaptation, and sustainability of agriculture in India: A bibliometric review. Heliyon, 2024, 10(8), e29586. DOI: 10.1016/j.heliyon.2024.e29586
[91] Wang Z, Schaaf CB, Sun Q, Shuai Y, Román MO. Capturing rapid land surface dynamics with Collection V006 MODIS BRDF/NBAR/Albedo (MCD43) products. Remote Sensing of Environment, 2018, 207, 50-64. DOI: 10.1016/j.rse.2018.02.001
[92] Vishvendra Raj Singh B, Agarwal V, Sanwal V. Climatic shifts and vegetation response in Western India: A four-decade retrospective through GIS and multi-variable analysis. Oxford Open Climate Change, 2024, 4(1), kgae020. DOI: 10.1093/oxfclm/kgae020